Transition from a phosphate to niobate network structure in vitreous Nb₂O₅-NaPO₃

Philip S. Salmon ■ ②; Esther Girón Lange ③; Anita Zeidler ⑤; Henrik Bradtmüller ⑤; Laureano Ensuncho ⑤; Gabriel J. Cuello ⑤; Hellmut Eckert ⑥



J. Chem. Phys. 163, 144510 (2025) https://doi.org/10.1063/5.0290349





Articles You May Be Interested In

Assessing the network connectivity of modifier ions in metaphosphate glass melts: A dynamic light scattering study of Na-Zn mixtures

J. Chem. Phys. (October 2016)

The identification of molecular NaPO₃ and NaPO₂ by matrix isolation IR spectroscopy

J. Chem. Phys. (August 1980)

Rheological characterization of complex dynamics in Na-Zn metaphosphate glass-forming liquids

J. Chem. Phys. (August 2021)



Transition from a phosphate to niobate network structure in vitreous Nb₂O₅-NaPO₃

Cite as: J. Chem. Phys. 163, 144510 (2025); doi: 10.1063/5.0290349 Submitted: 11 July 2025 • Accepted: 19 September 2025 •







Published Online: 14 October 2025 Philip S. Salmon, 1,a) (D) Esther Girón Lange, 1,2 (D) Anita Zeidler, 1 (D) Henrik Bradtmüller, 3,4 (D)

AFFILIATIONS

- ¹ Department of Physics, University of Bath, Bath BA2 7AY, United Kingdom
- ²Institut Laue Langevin, 71 Avenue des Martyrs, 38042 Grenoble Cedex 9, France

Laureano Ensuncho. De Gabriel J. Cuello. De and Hellmut Eckert De Gabriel J. Cuello. De and Hellmut Eckert De Gabriel J. Cuello. De

- ³Department of Materials Engineering, Vitreous Materials Laboratory and Center for Research, Technology and Education in Vitreous Materials (CeRTEV), Universidade Federal de São Carlos, Rod. Washington Luis, km 235, CP 676, São Carlos 13565-905,
- ⁴Instituto de Física de São Carlos, Universidade de São Paulo, São Carlos SP 13566-590, São Paulo, Brazil

ABSTRACT

The structure of (Nb₂O₅)_x(NaPO₃)_{1-x} glasses was re-visited by combining neutron and high energy x-ray diffraction with Raman scattering over a wide composition range. The results were interpreted by reference to the phosphorus atom speciation found from a novel analysis of ³¹P magic angle spinning nuclear magnetic resonance spectra [Ensuncho et al., J. Am. Chem. Soc. 147, 31147 (2025)]. The results indicate a distorted octahedral coordination environment for the Nb atoms across the composition range. The measured x-dependence of (i) the mean numbers of non-bridging oxygen (NBO) atoms and P-O-P and P-O-Nb connections per phosphate group, and (ii) the fraction of oxygen atoms in Nb-O-Nb connections, are described by a self-consistent analytical model in which there is a preferential formation of heteronuclear P-O-Nb bonds within a network structure formed by 4- and 6-coordinated P and Nb atoms, respectively, such that P-O-P connections are absent when the niobia content exceeds $x \sim 0.22$. At smaller x, the non-bridging oxygen atoms are distributed among the P- and Nb-centered polyhedral units. The model provides a connectivity density that accounts for the rapid increase in the glass transition temperature with increasing Nb₂O₅ content and shows that the enhancement to the non-linear optical properties for x > 0.2 is related to a more rapid increase with x in the fraction of oxygen atoms involved in polarizable Nb-O-Nb connections. The methodology also suggests that the dissolution rate measured for the $(Nb_2O_5)_x(Na_2O)_{0.4}(P_2O_5)_{0.6-x}$ glass series is dependent on the proportion of P-O-P linkages.

© 2025 Author(s). All article content, except where otherwise noted, is licensed under a Creative Commons Attribution-NonCommercial 4.0 International (CC BY-NC) license (https://creativecommons.org/licenses/by-nc/4.0/). https://doi.org/10.1063/5.0290349

I. INTRODUCTION

The $(Na_2O)_x(P_2O_5)_{1-x}$ $(0 \le x \le 1)$ binary is an exemplar phosphate glass-forming system in which the addition of the network modifier Na₂O to the network former P₂O₅ creates non-bridging oxygen (NBO) atoms to compensate the charge on the Na⁺ ions. ¹ This addition leads to a predictable depolymerization of the phosphate network.² For example, the P³ units of P₂O₅ (x = 0) are replaced by P² units for the metaphosphate composition NaPO₃ (x = 0.5), where the superscripts denote the number of bridging oxygen (BO) atoms per PO₄ tetrahedron. Such materials can be used as the host for Nb₂O₅, leading to a series of chemically stable glasses with an enhanced glass-transition temperature, high refractive index, and non-linear optical properties, which opens up

the possibility of innovative applications in optical waveguiding.^{3–8} Importantly, the non-linearity is achieved without the incorporation of toxic components such as lead, which has a beneficial environmental and health impact.

To optimize the material properties, it is important to know their relationship with the glass structure. Here, the coordination environments of phosphorus and sodium can be probed by solidstate ³¹P and ²³Na nuclear magnetic resonance (NMR) spectroscopy, respectively. However, the application of this method to niobium is hampered by the large electric quadrupole moment (nuclear spin I = 9/2) of the only stable isotope ⁹³Nb. In crystalline niobiumcontaining systems, this element can take coordination numbers from 4 to 8, where six-coordination is the dominant configuration with a broad distribution of Nb-O bond lengths (mean minimum

^{a)}Author to whom correspondence should be addressed: p.s.salmon@bath.ac.uk

of 1.944 Å and mean maximum of 2.046 Å) about a mean value of 1.993 Å.9 Based on work using model compounds, a 93Nb chemical shift scale has been proposed. 10 According to this scale, the measured ⁹³Nb chemical shifts for, e.g., $(Nb_2O_5)_x(NaPO_3)_{1-x}$ glasses with x > 0 suggest that Nb is six-coordinated.^{3,4} However, as for other nuclei with significant quadrupole moments in disordered materials, the assignment of NMR signals to coordination numbers in glasses based on chemical shift scales from crystalline model compounds may not always be reliable: There is excessive linebroadening of the NMR signal due to a distribution of interaction strengths of the nucleus with the electric field gradients present in locally distorted environments and different chemical shifts can be consistent with the same coordination number. 11 Thus, the composition dependence of the Nb coordination environment in phosphate glasses must be considered to be a basic but unknown quantity.

The purpose of this paper is to combine neutron and highenergy x-ray diffraction with Raman spectroscopy to investigate the structure of four glasses along the (Nb₂O₅)_x(NaPO₃)_{1-x} pseudobinary tie-line, with x = 0.025, 0.1, 0.2, and 0.4, which span the entire glass-forming region. A particular objective is to find the average Nb-O coordination number and the distribution of Nb-O distances and their dependence on the glass composition. The results are combined with those obtained from solid-state NMR spectroscopy¹² to build a comprehensive understanding of the structural changes that accompany the transition from a phosphate to a niobate network structure. An analytical model is developed for rationalizing the structural changes that occur.

This paper is organized as follows: the essential diffraction theory is given in Sec. II, and the experimental information is described in Sec. III; the results are presented in Sec. IV and are discussed in Sec. V with the aid of analytical models for the glass structure in which the NBO atoms are either (i) associated with the P atoms alone or (ii) distributed between the P and Nb atoms; and conclusions are provided in Sec. VI.

II. DIFFRACTION THEORY

In a neutron or x-ray diffraction experiment on glass, the measured diffraction pattern can be represented by the total structure factor, 13

$$S(k) = 1 + \sum_{\alpha} \sum_{\beta} W_{\alpha\beta}(k) \left[S_{\alpha\beta}(k) - 1 \right], \tag{1}$$

where k is the magnitude of the scattering vector. The structural information is contained in the partial structure factors $S_{\alpha\beta}(k)$ for the chemical species α and β . These functions are weighted by the factors $W_{\alpha\beta}(k) = c_{\alpha}c_{\beta}w_{\alpha}(k)w_{\beta}(k)/|\langle w(k)\rangle|^2$, where $c_{\alpha} = N_{\alpha}/N$ is the atomic fraction of chemical species α , N_{α} is the number of atoms of chemical species α , N is the total number of atoms, and $w_{\alpha}(k)$ denotes the scattering amplitude of chemical species α. In neutron and x-ray diffraction, the amplitudes correspond to the k-independent coherent neutron scattering lengths b_{α} and the k-dependent x-ray atomic form-factors $f_{\alpha}(k)$, respectively. The mean scattering amplitude is given by $\langle w(k) \rangle = \sum_{\alpha} c_{\alpha} w_{\alpha}(k)$. In the following, the subscripts "N" and "X" will refer to neutron and x-ray diffraction, respectively.

The corresponding real-space information is given by the total pair-distribution function,

$$D'(r) = \frac{2}{\pi} \int_0^{\infty} dk \ k[S(k) - 1] M(k) \sin(kr) = D(r) \otimes M(r), \quad (2)$$

where r is a distance in real space and \otimes denotes the onedimensional convolution operator. The modification function M(k)originates from the truncation of the measured S(k) function at a finite value k_{max} and takes the form of the step function M(k) = 1for $k \le k_{\text{max}}$ and M(k) = 0 for $k > k_{\text{max}}$. The desired structural information is contained in D(r), which is convoluted with M(r), the Fourier transform of M(k), unless k_{max} is sufficiently large that the oscillations in S(k) are not truncated. In this case, the unmodified function measured in neutron diffraction is given by

$$D_{\rm N}(r) = 4\pi \rho_0 \ r \sum_{\alpha} \sum_{\beta} W_{\alpha\beta} [g_{\alpha\beta}(r) - 1], \tag{3}$$

where ρ_0 is the atomic number density, $g_{\alpha\beta}(r)$ is the partial pair-distribution function for the chemical species α and β , $W_{\alpha\beta} = c_{\alpha}c_{\beta}b_{\alpha}b_{\beta}/|\langle b\rangle|^2$, and $\langle b\rangle = \sum_{\alpha}c_{\alpha}b_{\alpha}$.

Each peak i in $rg_{\alpha\beta}(r)$ can be represented by the Gaussian

$$p_{\alpha\beta}^{i}(r) = \frac{1}{4\pi\rho_0} \frac{\bar{n}_{\alpha}^{\beta}(i)}{c_{\beta}^{i} r_{\alpha\beta}^{i}} \frac{1}{\sqrt{2\pi}\sigma_{\alpha\beta}^{i}} \exp\left[-\frac{(r - r_{\alpha\beta}^{i})^{2}}{2(\sigma_{\alpha\beta}^{i})^{2}}\right], \tag{4}$$

with position $r_{\alpha\beta}^i$, standard deviation $\sigma_{\alpha\beta}^i$, and coordination number $\bar{n}_{\alpha}^{\beta}(i)$ of chemical species β around α . In neutron diffraction, a weighted sum of these Gaussian functions, convoluted with M(r), is fitted to $D'_{N}(r)^{14}$ using R_{χ} as a measure of the goodness-of-fit. In x-ray diffraction, the contribution of $p_{\alpha\beta}^{l}(r)$ toward $S_X(k) - 1$ can be found and, after applying the relevant weighting factor $(2 - \delta_{\alpha\beta})W_{\alpha\beta}(k)$, it is Fourier transformed to real space using the same M(k) function as employed for the experimental data. A sum of these Fourier transforms is then fitted to $T'_{\rm X}(r) = T_{\rm X}(r) \otimes M(r)$ using the program PXFIT, where $T_{\rm X}(r)$ $\equiv D_{\rm X}(r) + T_0(r)$ and $T_0(r) = 4\pi\rho_0 r$. The x-ray results are presented as $D_{\rm X}'(r) = [T_{\rm X}(r) - T_0(r)] \otimes M(r) = T_{\rm X}'(r) - 4\pi\rho_0 r$ to facilitate a direct comparison with the neutron diffraction data.

III. EXPERIMENT

A. Sample preparation and characterization

Glassy $(Nb_2O_5)_x(NaPO_3)_{1-x}$ $(0 \le x \le 0.4)$ samples were synthesized by a conventional melt-quenching technique using Nb₂O₅ (CBMM, Brazil, >99.99%) and NaPO₃ (Sigma Aldrich, 65-70 wt. % P₂O₅) as starting materials. Powders were dried in a muffle furnace at 120 °C for 24 h before mixing in their respective molar ratios via ten iterations of 1 min duration in a FlackTek Speedmixer operating at 1400 rpm. Each batch of homogenized powder of mass ~5 g was placed into a zirconia crucible and melted for 30 min at a temperature ranging from 850 to 1150 °C, depending on the Nb₂O₅ content. The melt was rapidly quenched by pouring onto a flat steel plate and punching with a second steel plate. The quenched glasses were of 1-2 mm thickness and were clear and transparent. They were colorless for $x \le 0.05$, had a blue tint for $0.075 \le x \le 0.15$, and had a

yellow tint for $x \ge 0.20$. The glass compositions were measured using wavelength dispersive x-ray fluorescence spectroscopy (WD-XRF) (Table I). The measured ZrO₂ content originating from the crucible material was small at 0.05-0.30 mol. %.12 The relatively low x-ray emission energy of Na leads to the greatest uncertainty regarding its content in the glass. The overall precision of the measurements was about ± 1 mol. %. In the following, the glasses will be referred to by their nominal compositions, but all parameters were calculated using the measured compositions after neglecting the ZrO₂ content.

Polycrystalline NbOPO4 was prepared using the procedure described elsewhere.¹⁷ 4 g of NbCl₅ was dissolved in 400 ml of 37% by weight hydrochloric acid. An over-stoichiometric amount of phosphoric acid was then added dropwise. After a few minutes of stirring, the resulting precipitate was kept at 80 °C for 12–14 h. It was then neutralized by adding ammonia solution until the pH reached a value of about 7, washed with distilled water, centrifuged several times, and dried overnight at 80 °C. Finally, the powder was kept at 900 °C for 12 h.

Polycrystalline NaNbO₃ was prepared by a conventional solidstate reaction method using Na₂CO₃ (Alfa Aesar, 98%) and Nb₂O₅ (CBMM, Brazil, >99.99%) as the starting materials. The powders were dried in an oven at 120 °C for 24 h, weighed to give the correct stoichiometric ratio, and ball milled with ethanol at 360 rpm for 24 h. Finally, the mixture was calcined at 950 °C for 4 h. 14

Polycrystalline Na₄Nb₈P₄O₃₂ was prepared from stoichiometric amounts of Na₂CO₃ (Alfa Aesar, 98%), (NH₄)₂HPO₄ (Sigma-Aldrich, >98%), and Nb₂O₅ (CBMM, Brazil, >99.99%) using a two-stage heating method (500 °C for 12 h, 1030 °C for 24 h), followed by slow quenching to room temperature.¹⁹

The amorphous vs crystalline states of the glass samples and model compounds, respectively, were verified using powder xray diffraction using a Rigaku Ultima IV diffractometer with filtered Cu-Kα radiation (wavelength 1.5418 Å) in Bragg-Brentano scattering geometry. A scattering angle 2θ range of 10° – 80° was probed at room temperature by employing a step size of 0.67° and an integration time of 0.67 s. The x-ray diffraction pattern measured for Na₄Nb₈P₄O₃₂ indicated a phase pure material consistent with the Inorganic Crystal Structural Database (ICSD) collection code 176659, which corresponds to the centrosymmetic space group $P2_1/c$. The other crystal structures are discussed in Sec. IV A.

The densities were measured either by using an Anton Paar micro-ultrapycnometer 1200e operating with helium gas or by Archimedes' method with isopropanol as the working fluid. In the former, 225-275 individual measurements were made for each sample and the mean and standard deviation were taken for the last ≈100 data points showing a minimal drift, indicating equilibrium with respect to the controlled temperature. In the latter, an average was taken of three measurements on different pieces of glass with the same composition. The glass transition temperature T_g was measured using a Netzsch DSC 204 Phoenix differential scanning calorimeter with a heating rate of 10 K min⁻¹ and a nitrogen atmosphere. Five separate measurements were made on each sample for x < 0.25 and a single measurement was made on each sample for larger Nb₂O₅ contents. The measured densities and T_g values are commensurate with those previously reported^{4,5} (Fig. 1).

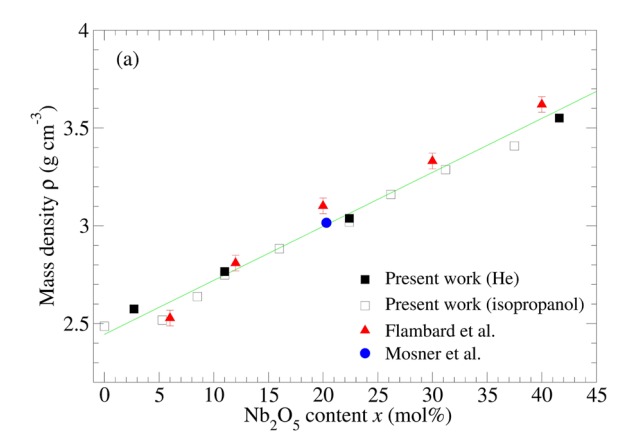
B. Neutron and x-ray diffraction

The instrument D4c at the Institut Laue-Langevin²⁰ was used for the neutron diffraction work with an incident wavelength of 0.4978(1) Å. The glass samples were coarsely ground and the crystalline $NbOPO_4$ and $NaNbO_3$ standards were finely ground. The samples were loaded into vanadium containers with an inner diameter of either 6.8 mm (x = 0.025) or 4.8 mm (all other samples) and wall thickness of 0.1 mm. Diffraction patterns were collected for each sample in its container at room temperature (~25°C), the empty container, the empty instrument, and a

TABLE I. Composition, mass density ρ , number density ρ_0 , molar volume V_{mol} per atom, and glass transition temperature T_{g} of the $(Nb_2O_5)_x(NaPO_3)_{1-x}$ glasses. The composition was measured using x-ray fluorescence (XRF) spectroscopy, which separated out the mole fraction contributions from Nb_2O_5 ($x_{Nb_2O_5}$), Na_2O (x_{Na_2O}), and P_2O_5 ($x_{P_2O_5}$). The density was measured at 22.3(1)°C.

x (nominal)	$x_{\mathrm{Nb}_2\mathrm{O}_5}$ (XRF)	$x_{\text{Na}_2\text{O}}$ (XRF)	$x_{P_2O_5}$ (XRF)	$\rho~({\rm g~cm}^{-3})$	$\rho_0(\mathring{\rm A}^{-3})$	$V_{\rm mol}~({\rm cm}^3)$	$T_{\rm g}$ (°C)
0	0	0.553	0.447	2.486(2)	0.073 35(6)	8.210(7)	281(5)
0.025	0.027	0.538	0.435	$2.575(2)^{a}$	0.073 51(5)	8.192(6)	309(5)
0.050	0.053	0.526	0.421	2.518(2)	0.06975(6)	8.634(7)	332(5)
0.075	0.085	0.487	0.428	2.638(5)	0.07069(13)	8.519(16)	356(5)
0.100	0.110	0.473	0.417	2.749(6)	0.071 82(16)	8.385(18)	376(5)
				$2.766(2)^{a}$	0.072 27(5)	8.333(6)	
0.150	0.160	0.444	0.396	2.883(3)	0.071 84(7)	8.383(9)	433(5)
0.200	0.224	0.406	0.370	3.019(5)	0.071 23(12)	8.455(14)	502(5)
				$3.038(2)^{a}$	0.07167(4)	8.403(5)	
0.250	0.262	0.398	0.340	3.160(6)	0.072 19(14)	8.343(16)	548(5)
0.300	0.312	0.367	0.321	3.287(5)	0.072 40(11)	8.317(13)	592(5)
0.350	0.375	0.327	0.298	3.408(2)	0.07200(4)	8.364(5)	626(5)
0.400	0.416	0.303	0.281	3.551(3) ^a	0.073 14(6)	8.234(7)	652(5)

^aObtained from He pycnometry



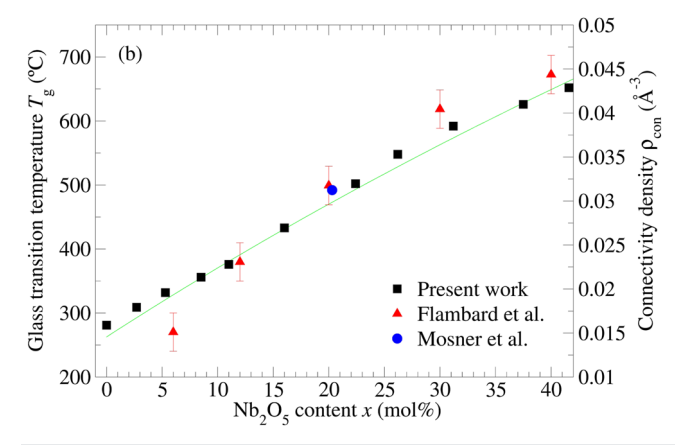


FIG. 1. Composition dependence of (a) the mass density and (b) the glass transition temperature from the present work, Flambard *et al.*⁴ and Mošner *et al.*⁵ The vertical lines represent the error bars, which are often smaller than the symbol size. In panel (a), the green solid curve shows a straight line fit to the data. In panel (b), the green curve shows the composition dependence of the connectivity density calculated from Eq. (22).

cylindrical vanadium rod of diameter 6.08 mm for normalization purposes. The datasets were analyzed by employing the method described elsewhere²¹ using coherent neutron scattering lengths of $b_{\rm Na} = 3.63(2)$ fm, $b_{\rm P} = 5.13(1)$ fm, $b_{\rm Nb} = 7.054(3)$ fm, and $b_{\rm O} = 5.803(4)$ fm. ^{22,23}

Beamline ID15A at the European Synchrotron Radiation Facility²⁴ was used for the x-ray diffraction work with an incident photon energy of 98 keV. Finely powdered samples were loaded into cylindrical polyimide capillaries of inner diameter 1.003 mm and wall thickness 0.051 mm. The beam was collimated to illuminate the central part of a capillary, and the scattered photons were detected using a DECTRIS Pilatus3 X CdTe 2M detector, which was placed at a distance of 325 mm from the sample as found from the diffraction pattern measured for a crystalline CeO₂ standard. Diffraction patterns were collected for each sample in its container at room temperature, an empty container, and the empty instrument. The datasets were analyzed by employing the method described elsewhere²⁵ using neutral atom x-ray form-factors.²⁶

C. Raman spectroscopy

Raman spectra were measured using a WITec Alpha 300 Raman microscope system with a laser excitation wavelength of 514 nm and 10 mW power.

IV. RESULTS

A. Diffraction: Crystal structure

Figure 2 shows the measured neutron and x-ray S(k) functions for the crystalline materials. The Bragg peaks are sharpest in the x-ray diffraction work because the diffractometer setup led to an enhanced k-space resolution function. The corresponding D'(r) functions are shown in Figs. 3 and 4. The functions were fitted by reference to the appropriate crystal structure. Here, the mean bond distances $\tilde{r}_{\alpha\beta}$ and coordination numbers $\tilde{n}_{\alpha}^{\beta}$ for a given chemical species α , over a specified distance range, were found by taking into account the coordination environment of each of the different crystallographic sites for that chemical species and the number of those sites present within the unit cell.

The crystal structure of NbOPO₄ was identified as the tetragonal phase with space group $P4/n^{27}$ by powder x-ray diffraction using Cu K α radiation, corresponding to the ICSD collection code 24110. In this structure, chains of corner-sharing octahedral NbO₆ units are linked together by tetrahedral PO₄ units, i.e., each NbO₆ unit is connected to 2 other NbO₆ units along the chain direction and to 4 PO₄ units. The NbO₆ units have four oxygen atoms with an Nb–O bond length of 1.969(9) Å and are distorted along the chain direction to give one shorter Nb–O bond length of 1.783(12) Å and one longer

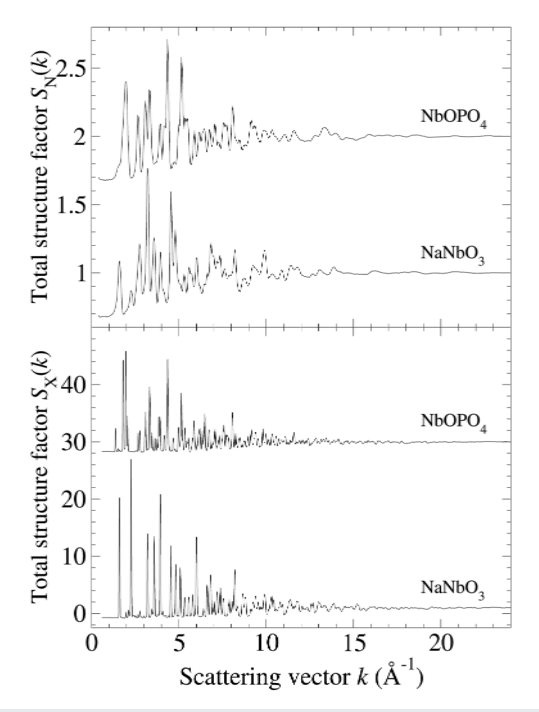


FIG. 2. Measured neutron and x-ray S(k) functions for crystalline NbOPO $_4$ and NaNbO $_2$

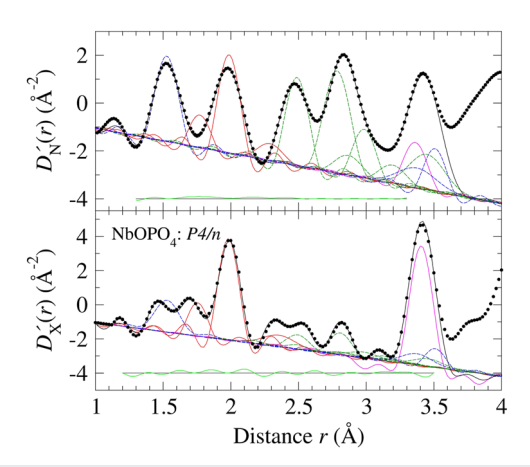


FIG. 3. Fitted $D'_{N}(r)$ and $D'_{X}(r)$ functions for crystalline NbOPO₄. In each panel, the filled circles represent the measured function; the black solid curve represents the fitted function; and the other curves represent the contributions from the P-O (blue broken curves), Nb-O (red solid curves), O-O (green broken curves), and Nb-P (magenta solid curve) correlations. The displaced green solid curve represents the residual.

Nb-O bond length of 2.321(12) Å. Each PO₄ motif forms a regular tetrahedron with a P-O bond length of 1.528(9) Å and is connected to 4 NbO₆ units. Figure 3 shows that the measured $D'_{N}(r)$ and $D'_{X}(r)$ functions are consistent with the P4/n crystal structure. The fitted parameters are summarized in Table II. The bond lengths are within 1.5% of the mean values found from crystallography. The number density measured using helium pycnometry $\rho_0 = 0.0807(4) \text{ Å}^{-3}$ is $\simeq 3.5\%$ smaller than the crystallographic value of $\rho_0 = 0.0836 \text{ Å}^{-3}.^{27}$

The crystal structure of the perovskite NaNbO3 could not be unambiguously determined by powder x-ray diffraction using Cu $K\alpha$ radiation because of the similarity between the measured diffraction patterns for the orthorhombic polymorphs with space groups Pbcm and P21ma.²⁸ Both structures are based on corner-sharing octahedral NbO₆ units with 4 Nb-O bond lengths of 1.958(19) or 1.933(51) Å and 2 longer Nb-O bond lengths of 2.034(40) or 2.096(7) Å, respectively (Table II). For both crystal structures, the Na-O coordination number is given by $\bar{n}_{Na}^{O} = 12$ and the Na-O bond lengths are distributed over the range of 2.286–3.229 Å (*Pbcm*) or 2.338-3.337 Å (P21ma). The structure-property relationships of such perovskites depend on (i) the displacement of the Na⁺ and Nb⁵⁺ ions from their (high-temperature) sites and (ii) the distortion of the octahedral NbO₆ units.²⁹ Figure 4 shows that the measured $D'_{N}(r)$ and $D'_{X}(r)$ functions cannot be fitted simultaneously using either the Pbcm or P21ma space group structure, which may indicate the presence of another phase. The fitted parameters are summarized in Table II, where the peak positions are within 4% of the mean bond lengths found from crystallography. The number density measured using helium pycnometry $\rho_0 = 0.0830(4) \text{ Å}^{-3}$ is $\simeq 1\%$ smaller than the crystallographic value of $\rho_0 = 0.0841 \text{ Å}^{-3}$ (*Pbcm*) or $\rho_0 = 0.0839 \text{ Å}^{-3}$

B. Summary of solid-state ³¹P NMR results

This section summarizes the main results from a prior NMR characterization study of the Nb₂O₅-NaPO₃ glasses,¹² which

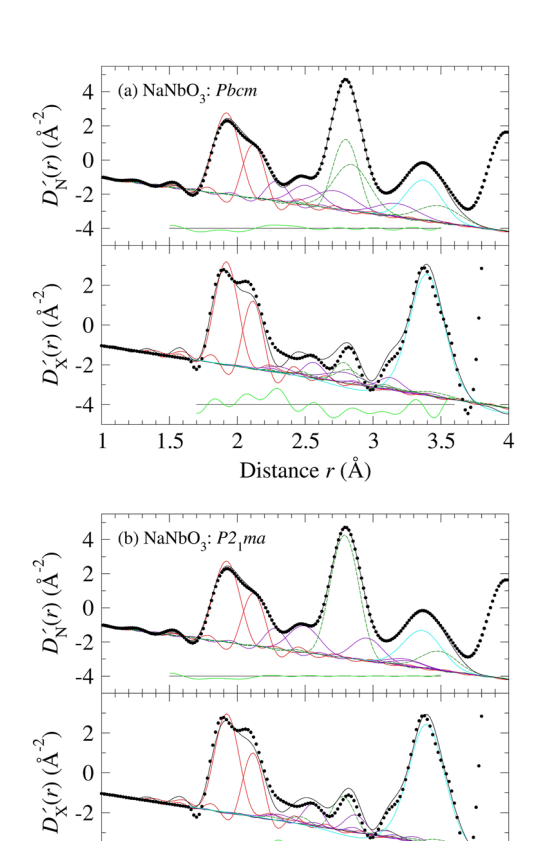


FIG. 4. Fitted $D'_{N}(r)$ and $D'_{X}(r)$ functions for crystalline NaNbO₃ assuming either (a) the Pbcm or (b) the P21ma space group. In each panel, the filled circles represent the measured function; the black solid curve represents the fitted function; and the other curves represent the contributions from the Nb-O (red solid curves), Na-O (violet solid curves), O-O (green broken curves), and Na-Nb (cyan solid curve) correlations. The displaced green solid curve represents the residual.

2.5

Distance r (Å)

3

3.5

1.5

provide useful constraints for the analysis of the diffraction data. ³¹P magic angle spinning (MAS) NMR experiments were performed on exactly the same set of glass samples as used for the diffraction and Raman experiments. Table III lists the phosphorus atom speciation P_{mNb}^n obtained from those experiments, where n denotes the total number of BO atoms in P-O-P and P-O-Nb connections and m denotes the number of these BO atoms in P-O-Nb connections alone. The results provide the P-BO coordination number $\bar{n}_{\rm P}^{\rm BO}$ and the P-NBO coordination number $\bar{n}_{\rm P}^{\rm NBO}$, which is equivalent to the mean number of NBO atoms per P atom $N_{\rm NBO}/N_{\rm P}$. They also deliver the mean number of P-O-P connections per P atom N_{POP}/N_P and the mean number of P-O-Nb connections per P atom $N_{\rm PONb}/N_{\rm P}$. There is an evolution in the distribution of species, from predominantly metaphosphate $P_{0 \text{ Nb}}^2$ or $[P\emptyset_{2/2}O_2]^-$ motifs at small x, where Ø denotes a bridging oxygen atom, to a distribution of P_{3Nb}^3 and P_{4Nb}^4 motifs at the largest x values that reflects an increased degree of network polymerization. For the highest niobia content glasses ($x \ge 0.25$), at least three P-O-Nb connections are formed and P-NBO connections remain but P-O-P linkages are absent.

TABLE II. Peak parameters obtained from the fitted $D'_{X}(r)$ and $D'_{X}(r)$ functions for crystalline NbOPO₄ and NaNbO₃ compared to the mean bond lengths found from crystallography. The neutron diffraction (ND) and x-ray diffraction (XRD) datasets for NbOPO₄ were fitted by assuming the space group P4/n,²⁷ and the datasets for NaNbO₃ were fitted by assuming either the space group Pbcm or the space group P2₁ma.²⁸ The coordination numbers for the peaks were set at the values found from crystallography. The $R_{\rm Y}$ values correspond to the fitted ranges shown in Figs. 3 and 4. The errors associated with $r_{\alpha\beta}$ and $\sigma_{\alpha\beta}$ are typically ± 0.010 and ± 0.015 Å, respectively.

		Crystalle	ography	N	ID		XRD		
Crystal	α-β	$\bar{r}_{\alpha\beta}$ (Å)	$ar{n}_lpha^eta$	$\bar{r}_{\alpha\beta}$ (Å)	$\sigma_{\alpha\beta}$ (Å)	R_χ	$\bar{r}_{\alpha\beta}$ (Å)	$\sigma_{\alpha\beta}$ (Å)	R_{χ}
NbOPO ₄	P-O	1.528	4	1.527	0.059	0.031	1.530	0.071	0.051
	Nb-O	1.783	1	1.773	0.018		1.756	0.035	
		1.969	4	1.986	0.049		1.984	0.054	
		2.321	1	2.290	0.078		2.357	0.118	
	O-O	2.495	2.4	2.490	0.060		2.495	0.064	
		2.794	4	2.786	0.089		2.809	0.062	
		2.850	0.8	2.868	0.090		2.840	0.120	
		2.977	1.6	2.986	0.061		2.981	0.098	
	Nb-P	3.398	4	3.363	0.065		3.407	0.063	
NaNbO ₃	Nb-O	1.958	4	1.921	0.086	0.062	1.920	0.079	0.204
Pbcm		2.034	2	2.120	0.042		2.115	0.039	
	Na-O	2.344	1.5	2.293	0.035		2.313	0.080	
		2.589	3	2.510	0.110		2.565	0.039	
		2.787	4	2.720	0.150		2.790	0.117	
		3.101	3.5	3.180	0.150		3.130	0.065	
	O-O	2.775	4	2.800	0.084		2.786	0.038	
		2.830	4	2.842	0.132		2.821	0.079	
		3.448	2	3.490	0.150		3.449	0.112	
	Na-Nb	3.382	8	3.375	0.130		3.399	0.120	
NaNbO ₃	Nb-O	1.933	4	1.922	0.086	0.047	1.923	0.083	0.191
$P2_1ma$		2.096	2	2.120	0.045		2.116	0.047	
	Na-O	2.360	1.5	2.280	0.035		2.311	0.079	
		2.578	4	2.493	0.108		2.561	0.034	
		2.885	4	2.958	0.107		2.870	0.050	
		3.097	1.5	3.238	0.123		3.103	0.042	
		3.337	1	3.267	0.100		3.308	0.115	
	O-O	2.803	8	2.792	0.100		2.782	0.060	
		2.456	2	2.490	0.131		3.483	0.084	
	Na-Nb	3.385	8	3.364	0.140		3.396	0.124	

The ³¹P MAS NMR spectra were interpreted with the aid of the results obtained from a separate set of dipolar NMR experiments.¹² For each glass composition, the number of P-O-P linkages per P atom was probed independently via the \$^{31}P-^{31}P\$ dipole-dipole interactions measured using both ³¹P static spin echo decay (SED) and ³¹P constant-time double-quantum dipolar recoupling enables nuclear alignment reduction (CT DQ-DRENAR) experiments. The results show a continuous reduction in the fraction of P-O-P linkages with increasing x and the absence of these linkages when x > 0.20. The P-O-Nb linkages were probed via the 31 P- 93 Nb dipole-dipole interactions measured using unprecedented ³¹P{⁹³Nb} wideband uniform rate with smooth truncation (WURST) rotational-echo saturation-pulse double-resonance (W-RESPDOR) experiments. The method provides a quantitative estimate of $N_{\rm PONb}/N_{\rm P}$, and the extracted values are compared to those found from the $^{31}{\rm P}$ MAS NMR experiments in Table III. For

each glass, the number of P-O-Nb connections deduced from the results was found to be similar to the number of Nb-O-P connections deduced from independent ⁹³Nb{³¹P} rotational echo double resonance (REDOR) experiments.

It is important to note that the Na₂O:P₂O₅ ratio of 0.553:0.447 measured by WD-XRF (Table I) for the x = 0 glass requires a P_{0Nb}^2 : P_{0Nb} ratio of 0.763:0.237 to balance the positive charge on the Na⁺ ions (the charges on the P_{0Nb}^2 and P_{0Nb}^1 motifs are -1 and -2, respectively, in units of the elementary charge). In comparison, the P_{0Nb}^{2} : P_{0Nb}^{1} ratio of 0.90(1):0.10(1) found from the peak areas in the measured ³¹P MAS NMR spectrum (Table III) is significantly different. The latter provides a quantitatively rigorous analysis and indicates a Na₂O: P_2O_5 ratio of 0.524(2):0.476(2), i.e., for the x = 0composition, the Na/P ratio is 1.10(1) rather than the value of $\simeq 1.24$ found from WD-XRF. The Na:P ratios found from the XRF experiments are, therefore, likely to be overestimates that originate from

found from the ³¹P MAS NMR experiments of Ensuncho et al. ¹² The corresponding P–NBO and P–BO coordination numbers **TABLE III.** Phosphorus atom speciation P_m^n TABLE III. Phosphorus atom speciation $P_{mNb}^{\prime\prime}$ found from the $^{\prime\prime}P$ MAS NMR experiments of Ensurcho et al. $^{\prime\prime}$ the corresponding P-NBO and P-BO coordination numbers are given, along with a breakdown of the P-BO connections into the ratios N_{POP}/N_P and N_{PONb}/N_P . The O-O coordination number for the shortest O-O nearest-neighbor distances of $\simeq 2.52$ Å, which are associated with the oxygen atoms in the phosphate groups, was calculated using Eq. (5). The N_{PONb}/N_P values from $^{31}P\{^{93}Nb\}$ W-RESPDOR experiments are also listed. 12 The error on the fractions of P_{mNb}^{n} species is ± 0.01 , and the error on the W-RESPDOR results is ± 0.1 . The full precision is given to minimize rounding errors in the analytical models.

x	P_{0Nb}^1	P_{0Nb}^2	P_{1Nb}^2	P_{2Nb}^3	P_{3Nb}^3	P_{4Nb}^4	$ar{n}_{ ext{P}}^{ ext{NBO}}$	$ar{n}_{ m P}^{ m BO}$	$N_{ m POP}/N_{ m P}$	$N_{ m PONb}/N_{ m P}$	$\bar{n}_{\mathrm{O}}^{\mathrm{O}}(\mathrm{short})$	$N_{\rm PONb}/N_{\rm P}^{\rm a}$
0	0.100	0.900					2.10	1.90	1.900		3.85	
0.025	0.042	0.725	0.233				2.04	1.96	1.725	0.233	3.67	0.22
0.05	0.026	0.506	0.344	0.125			1.90	2.10	1.507	0.594	3.49	0.60
0.075	0.016	0.304	0.363	0.317			1.70	2.30	1.304	0.997	3.37	1.09
0.10	0.016	0.209	0.411	0.363			1.65	2.35	1.208	1.137	3.22	1.22
0.15		0.030	0.310	0.350	0.310		1.34	2.66	0.720	1.940	3.12	2.0
0.20			0.158	0.152	0.690		1.16	2.84	0.310	2.532	2.63	2.4
0.25					0.950	0.050	0.95	3.05	0	3.050	2.39	
0.30					0.820	0.180	0.82	3.18	0	3.180	2.18	2.7
0.40	• • •		• • •	• • •	0.719	0.281	0.72	3.28	0	3.281	1.78	3.3

^aObtained from ³¹P{⁹³Nb} W-RESPDOR.

the difficulty in accurately measuring the bulk Na content of these materials from a near-surface analysis using the WD-XRF method (Sec. III A).

C. Diffraction: Glass structure

Figure 5 shows the measured neutron and x-ray total structure factors for the glassy materials. At a given composition, the contrast in shape originates from the difference in the weighting factors for the partial structure factors [see Eq. (1)], where the niobium pair-correlations receive a large weighting in the x-ray diffraction work. The corresponding total pair-distribution functions D'(r) are presented in Fig. 6 and show substantial changes with the glass composition. The functions were fitted by taking into account the information available from other experimental techniques.

In the crystalline metaphosphate NaPO₃, each P atom is bound to 2 NBO and 2 BO atoms, and the mean P-BO bond length of 1.609(11) Å is ≃9% longer than the mean P-NBO bond length of 1.478(6) Å.30 In crystalline NbOPO4, by comparison, each P atom makes 4 P-O-Nb connections, providing a P-O bond length of 1.528 Å²⁷ that is \simeq 3% longer than the P–NBO bond length in NaPO₃. In glassy NaPO₃, the contributions from the P-NBO and P-BO distances can be resolved in neutron diffraction experiments that employ a large cutoff $k_{\text{max}} = 45 \text{ Å}^{-1.31}$ In such experiments, the contributions from these connections are also discernible from the asymmetry of the measured nearest-neighbor P-O peak in $D'_{N}(r)$ for the x = 0.08 composition, but not for the compositions when $x \ge 0.12$. In the present work, the P-O peak in D'(r) at $\simeq 1.53$ Å was fitted accordingly. Two Gaussian functions were used to represent the P-NBO and P-BO nearest-neighbors for the $x \le 0.10$ glasses, with the corresponding coordination numbers fixed at the values found from the ³¹P NMR experiments (Table III). A single Gaussian function was used for the $x \ge 0.20$ glasses, with the P-O coordination number fixed at $\bar{n}_{\rm P}^{\rm O} = 4$, where the fraction of P-O-P linkages is small or zero and a small difference is expected between the P-O bond lengths for the P-NBO and P-O-Nb connections.

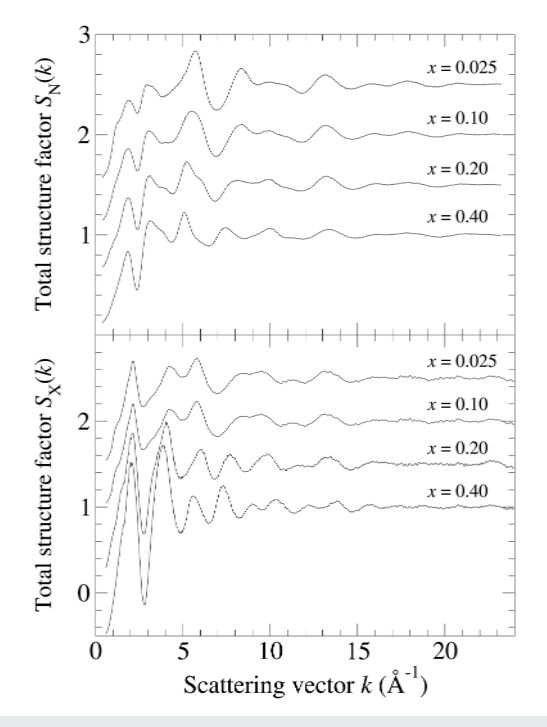


FIG. 5. Measured neutron and x-ray S(k) functions for the $(Nb_2O_5)_x(NaPO_3)_{1-x}$ glasses

As the niobia content of the glass increases from x = 0.025, a shoulder appears on the high-r side of the nearest-neighbor P-O peak in $D'_{X}(r)$ and grows in intensity. The second peak in both $D'_{\rm X}(r)$ and $D'_{\rm N}(r)$ at $\simeq 2.04$ Å also grows in intensity. These changes are attributed to the appearance of nearest-neighbor Nb-O correlations and the features were fitted accordingly. For the glasses with $x \ge 0.10$, allowance was also made for a third Nb-O peak at ≃2.28 Å.

 $D_{\mathbf{X}}^{\prime}(r)\left(\mathbf{\mathring{A}}^{-2}\right)$

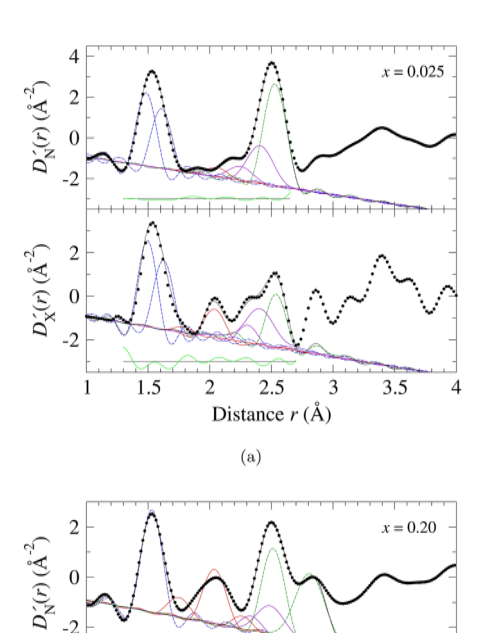
1.5

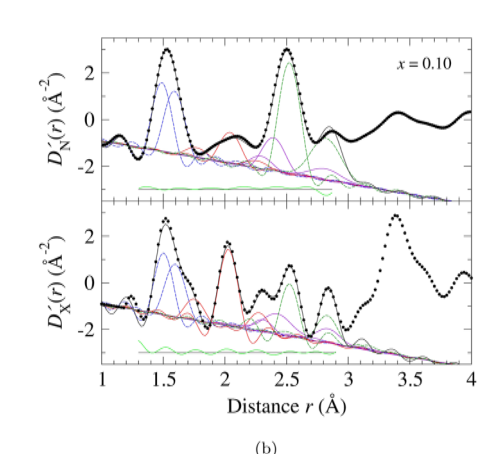
2.5

Distance r (Å)

3

3.5





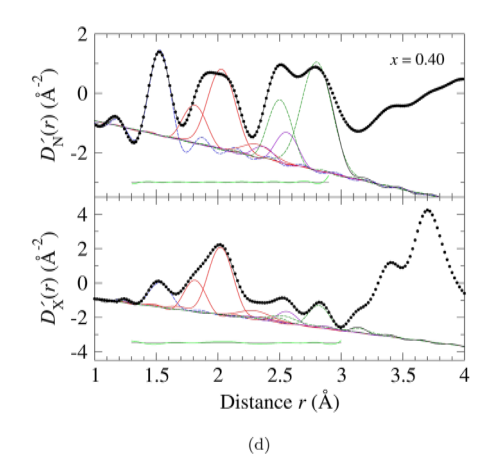


FIG. 6. Fitted $D'_{\rm N}(r)$ and $D'_{\rm X}(r)$ functions for the (a) x=0.025, (b) x=0.10, (c) x=0.20, and (d) x=0.40 glasses. In each panel, the filled circles represent the measured function; the black solid curve represents the fitted function; and the other curves represent the contributions from the P–O (broken blue curves), Nb–O (red solid curves), Na–O (violet solid curves), and O–O (green broken curves) correlations. The displaced green solid curve represents the residual

The peak in $D_{\rm X}'(r)$ and $D_{\rm N}'(r)$ at $\simeq 2.52$ Å will originate from the shorter O–O distances within or between the PO₄ motifs and not from the longer O–O distances associated with the niobiumor sodium-centered polyhedral units. The coordination number $\bar{n}_{\rm O}^{\rm O}({\rm short})$ for these short O–O distances can be found on the basis that (i) each NBO atom in a P–NBO connection or each BO atom in a P–O–Nb connection will have three nearest-neighbor oxygen atoms within a PO₄ group, and (ii) each BO atom in a P–O–P connection will have 6 nearest-neighbor oxygen atoms within the two adjoining PO₄ groups. Assuming that all the NBO species are bound to phosphorus atoms, and denoting the number of oxygen atoms in P–O–Nb and P–O–P connections by $N_{\rm O,PONb}$ and $N_{\rm O,POP}$, respectively, it follows that

$$\bar{n}_{O}^{O}(\text{short}) = \frac{1}{N_{O}} (3N_{NBO} + 3N_{O,PONb} + 6N_{O,POP})
= \left(3\frac{N_{NBO}}{N_{P}} + 3\frac{N_{PONb}}{N_{P}} + 6\frac{N_{POP}}{2N_{P}}\right) \frac{N_{P}}{N_{O}} = 12\frac{c_{P}}{c_{O}}.$$
(5)

The factor of 1/2 in the expression after the second equality avoids the double counting of the oxygen atoms in P-O-P connections, and the expression after the last equality follows from $\tilde{n}_{\rm P}^{\rm O} = (N_{\rm NBO} + N_{\rm PONb} + N_{\rm POP})/N_{\rm P} = 4$. Equation (5) gives the value

 $\bar{n}_{O}^{O}(\text{short}) = 4$ found for the x = 0 (metaphosphate) crystal structure³⁰ and reproduces the $\bar{n}_{O}^{O}(\text{short})$ values reported for the $(Nb_2O_5)_x(NaPO_3)_{1-x}$ glasses investigated in Ref. 31. It also provides the value $\bar{n}_{O}^{O}(\text{short}) = 1.5$ found for the x = 0.5 crystal structures of $Na_4Nb_8P_4O_{32}$ where all the phosphorus atoms form $P_{4\,\mathrm{Nb}}^4$ species. 19,32 Here, each of the oxygen atoms in a $P_{4\,\mathrm{Nb}}^4$ motif has three nearest-neighbor oxygen atoms within that motif but (i) the overall O-O coordination number for a specified distance range is obtained by averaging over all oxygen atom sites, and (ii) the O-O distances within, e.g., an octahedral NbO6 unit are much longer than 2.52 Å. For the x = 0.5 composition, only 50% of the oxygen atoms are bound to phosphorus atoms (Sec. V A), so the O-O coordination number for distances around 2.52 Å, averaged over all oxygen atoms, is given by $\bar{n}_{O}^{O}(\text{short}) = 0.5 \times 3 = 1.5$. In fitting the D'(r)functions, the short-distance O-O coordination numbers were fixed at the calculated values (Table III).

The Na–O nearest-neighbors are expected to first appear in D'(r) at distances around 2.3 Å. As in Ref. 31, their distribution was best represented by using two or more Gaussian functions.

Finally, each of the $D_{\rm X}'(r)$ functions also has a notable peak at $\simeq 2.82$ Å with a high-r boundary that approaches the density line $[D_{\rm X}'(r)=-4\pi\rho_0 r]$ limit for the x=0.20 and x=0.40 compositions. This feature was fitted by assuming significant contributions from

the O–O correlations for the x = 0.20 and x = 0.40 glasses and from the Na–O and O–O correlations for the x = 0.10 glass. An attempt to fit the peak for the x = 0.025 glass using a combination of Na–O and O-O correlations was unsuccessful as it led to large coordination numbers that could not be reconciled with the measured $D'_{N}(r)$ function. At this composition, there is, however, considerable overlap of the peak with the correlations at larger *r* values, such that the high-r peak boundary does not approach the density line limit. A benefit of fitting the feature in $D'_{\rm X}(r)$ at $\simeq 2.82$ Å is to constrain the peaks fitted at smaller r values.

The fitted $D'_{N}(r)$ and $D'_{X}(r)$ functions for the glasses are shown in Fig. 6, and the fitted parameters are listed in Table IV.

D. Raman spectroscopy

Figure 7 compares the Raman spectra for the glasses with those for crystalline NbOPO₄, NaNbO₃, and Na₄Nb₈P₄O₃₂, where the latter corresponds to the composition x = 0.5 on the $(Nb_2O_5)_x(NaPO_3)_{1-x}$ pseudo-binary tie-line. The spectrum for the Nb-free glass features a band with a maximum near 685 cm⁻¹, which arises from the symmetric stretching mode vibrations of the BO species within P-O-P linkages.³³ The band at 1170 cm⁻¹ signifies the vibrations of the NBO atoms in P2 groups,33 and its dominance indicates that these metaphosphate units are the majority species. In addition, there are small but noticeable bands at 1020

TABLE IV. Peak parameters obtained from the fitted $D'_{N}(r)$ and $D'_{X}(r)$ functions for the neutron diffraction (ND) and x-ray diffraction (XRD) experiments on the (Nb₂O₅)_x(NaPO₃)_{1-x} glasses. The total Nb–O and Na–O coordination numbers are also listed for the fitted r ranges. Fixed parameters are marked by an asterisk. The R_r values correspond to the fitted ranges shown in Fig. 6. The errors associated with $\bar{r}_{\alpha\beta}$, $\sigma_{\alpha\beta}$ and \bar{n}_{α}^{β} are typically ± 0.010 Å, ± 0.015 Å, and ± 0.10 , respectively.

				ND					XRD		
x	α-β	$\bar{r}_{\alpha\beta}$ (Å)	$\sigma_{\alpha\beta}$ (Å)	$ar{n}_lpha^eta$	$\bar{n}_{\alpha}^{\beta}(\mathrm{tot})$	R_{χ}	$\bar{r}_{\alpha\beta}$ (Å)	$\sigma_{\alpha\beta}$ (Å)	$ar{n}_lpha^eta$	$\bar{n}_{\alpha}^{\beta}(\mathrm{tot})$	R_{χ}
0.025	P-O	1.485	0.043	2.04*		0.038	1.494	0.038	2.04*		0.149
		1.610	0.055	1.96^{*}			1.625	0.051	1.96^{*}		
	Nb-O	1.820	0.040	0.72	6.3(3)		1.789	0.046	0.71	6.3(3)	
		2.060	0.065	5.60			2.041	0.073	5.59		
	Na-O	2.250	0.090	1.23	5.1(3)		2.310	0.043	0.99	4.8(3)	
		2.410	0.100	3.90			2.407	0.108	3.76		
	O-O	2.529	0.079	3.67*			2.539	0.065	3.67*		
0.10	P-O	1.490	0.035	1.88^{*}		0.058	1.505	0.033	1.88^{*}		0.092
		1.591	0.058	2.12*			1.596	0.062	2.12*		
	Nb-O	1.770	0.060	1.10	6.4(3)		1.754	0.060	1.02	6.2(3)	
		2.045	0.063	4.15			2.030	0.053	4.05		
		2.260	0.070	1.10			2.279	0.053	1.09		
	Na-O	2.294	0.070	0.95	5.5(3)		2.310	0.050	0.94	5.6(3)	
		2.395	0.080	2.90			2.425	0.107	2.79		
		2.815	0.120	1.60			2.836	0.084	1.84		
	O-O	2.524	0.068	3.22*			2.526	0.037	3.22*		
		2.820	0.120	2.10			2.831	0.069	2.49		
0.20	P-O	1.531	0.059	4.00*		0.035	1.537	0.053	4.00*		0.072
	Nb-O	1.750	0.073	1.23	6.3(3)		1.751	0.065	1.20	6.4(3)	
		2.040	0.080	4.25			2.028	0.064	4.36		
		2.263	0.045	0.81			2.280	0.052	0.79		
	Na-O	2.334	0.050	1.12	4.9(3)		2.312	0.050	0.94	4.6(3)	
		2.490	0.106	3.80			2.501	0.123	3.70		
	O-O	2.515	0.080	2.63*			2.525	0.030	2.63*		
		2.814	0.118	3.20			2.816	0.052	3.32		
0.40	P-O	1.530	0.050	4.00*		0.036	1.535	0.065	4.00*		0.038
	Nb-O	1.813	0.083	1.42	6.4(3)		1.815	0.074	1.40	6.4(3)	
		2.031	0.109	4.20	. ,		2.024	0.098	4.19		
		2.321	0.115	0.80			2.300	0.128	0.79		
	Na-O	2.369	0.051	1.20	5.5(3)		2.331	0.080	1.07	5.2(3)	
		2.560	0.077	4.30	. ,		2.563	0.047	4.14	. ,	
	0-0	2.505	0.088	1.78*			2.525	0.102	1.78*		
		2.804	0.122	4.60			2.820	0.066	4.48		

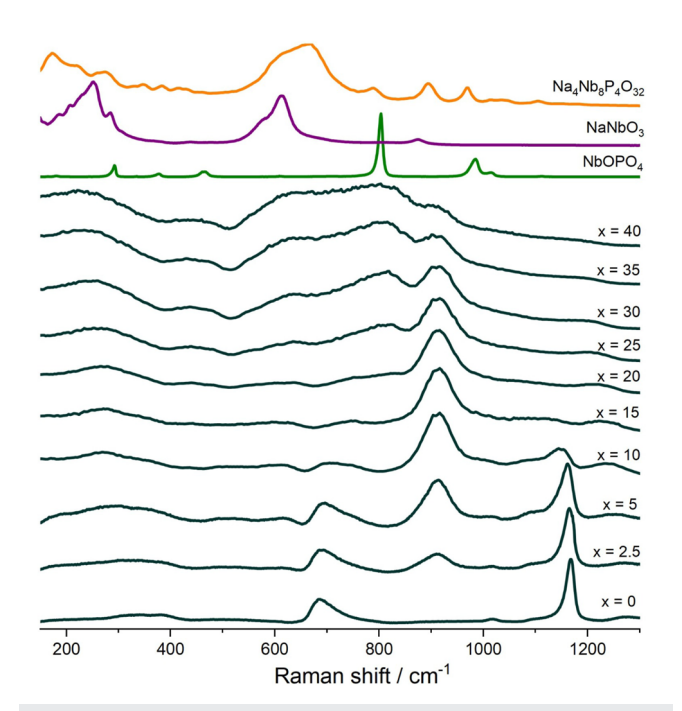


FIG. 7. Measured Raman spectra for crystalline Na₄Nb₈P₄O₃₂, NaNbO₃, and NbOPO $_4$ and for glassy $(Nb_2O_5)_x(NaPO_3)_{1-x}$. The ordinate axis represents the measured intensity in arbitrary units, and the spectra are stacked for clarity of presentation. In this figure, the x values are expressed in mol. %

and 1280 cm⁻¹, which are assignable to the stretching modes of the NBO atoms in P¹ and P² units, respectively.^{1,8,3}

The incorporation of niobium oxide produces notable composition-dependent changes to the glass spectra. For example, the band at 685 cm⁻¹, which arises from P-O-P linkages, shifts toward a larger wavenumber and diminishes in intensity, indicating a depolymerization of the phosphate network. This band is not discernible as a distinct feature when x > 0.10. In the glasses with $x \le 0.15$, a single band near 910 cm⁻¹ becomes dominant and has been attributed to the vibrational modes of isolated NbO₆ units,³⁴ i.e., distorted octahedral NbO6 motifs not linked to other NbO6 units. As discussed in Sec. V D, there may also be a contribution from the vibrations of non-bridging oxygen atoms bound to sixcoordinated Nb species. In the glasses with x > 0.15, an additional band appears at 820 cm⁻¹. Its position corresponds to that of the dominant Raman band observed for crystalline NbOPO₄, which features a network structure in which octahedral NbO6 species are corner-linked via bridging oxygen atoms to 4 PO_4 and 2 NbO_6 species.²⁷ Based on this comparison, the band at 820 cm⁻¹ is attributed to the vibrations of the O atoms within NbO6 polyhedral units connected via both Nb-O-P and Nb-O-Nb linkages.

Finally, a broad band at 630 cm⁻¹ develops for $x \ge 0.20$ and grows in intensity. The position of this band is close to that found for a prominent band in the spectrum for crystalline NaNbO3, which features a structure in which slightly distorted NbO6 units cornershare with 6 other NbO₆ units to form a three-dimensional network.³⁶ The band is, therefore, attributed to the vibrational modes of NbO₆ units connected predominantly to other NbO₆ units via

Nb-O-Nb linkages, and its growth indicates that the number of these connections increases with the niobium oxide content of the glass, as expected from probability considerations. The Raman spectrum for crystalline Na₄Nb₈P₄O₃₂, in which distorted NbO₆ units corner share with either (i) 3 NbO6 and 3 PO4 or (ii) 5 NbO6 and 1 PO $_4$ units, 19,32 supports a contribution to the region around 630–820 cm $^{-1}$ from the vibrations of O atoms within NbO $_6$ polyhedral units connected via both Nb-O-P and Nb-O-Nb corner-sharing linkages.

V. DISCUSSION

For the x = 0.025 and x = 0.10 compositions, the fitted P-O bond distances are commensurate with those found in previous diffraction work on Nb₂O₅-NaPO₃ glasses³¹ and on crystalline NaPO₃ in which the mean P-NBO and P-BO bond distances are 1.478(6) and 1.609(11) Å, respectively.³⁰ In this crystal, $\bar{n}_{Na}^{O} = 5$ and the mean Na-O distance is 2.406(66) or 2.445(42) Å depending on the crystallographic site, where the numbers in parentheses refer to the standard deviations. In comparison, $\bar{n}_{Na}^{O} \simeq 4.9(3)$ with a weighted mean distance $\bar{r}_{NaO} \simeq 2.38$ Å for the x = 0.025 glass.

For each glass, the results are consistent with the Nb⁵⁺ ions adopting a distorted octahedral coordination environment. For the x = 0.025 composition, there is a $\sim 1 + 5$ deformation of the octahedron, with the majority of Nb-O bond lengths appearing around 2.05(2) Å. For $x \ge 0.10$, the distortion is similar to that found for crystalline NbOPO₄, i.e., there is a ~1 + 4 + 1 deformation of the octahedron with one Nb-O bond length shorter and one bond length longer than the other four. This distribution is similar to that previously reported for the Nb₂O₅-NaPO₃ glass system.³¹

In crystalline NbOPO₄, the short and long Nb-O bonds correspond to Nb-O-Nb connections.²⁷ In crystalline (NbO)₂(P₄O₁₃), by comparison, each NbO₆ polyhedron has five corner-sharing tetrahedral PO₄ units plus one NBO atom.³⁷ A wide range of other conformations exist for the NbO₆ polyhedral units in niobium phosphate crystals. It is reported that the ⁹³Nb NMR shift is relatively insensitive to the distortion within an NbO₆ unit but sensitive to the identity of the next nearest-neighbors.³⁸ The chemical shift parameters reported from ⁹³Nb MAS NMR experiments on the glasses investigated in the present work indicate a variety of NbO6 units with different degrees of distortion.¹²

The overall results for the composition dependence of the molar volume V_{mol} (Fig. S1) show that this parameter decreases as the Nb₂O₅ content of the glass increases, and the connectivity of the network also increases by the formation of Nb-O-P and Nb-O-Nb linkages (Sec. V B).

A. Analytical model I (NBO atoms exclusively P-bonded) vs statistical model for the glass structure

An analytical model for the glass structure was developed to aid in the interpretation of the experimental results. The starting point is a network comprising all the phosphorus and niobium atoms and all the oxygen atoms, which are deemed to be either one-coordinated NBO or two-coordinated BO species. Higher coordinated oxygen atoms are not considered: Although they are common in the structure of pure transition metal oxides including Nb₂O₅,³⁹ they are not included because of their absence in the crystalline model compounds NbOPO4 and Na4Nb8P4O32. The fraction of NBO atoms is given by40

$$f_{\rm NBO} = \frac{N_{\rm NBO}}{N_{\rm O}} = 2 - \frac{c_{\rm P}}{c_{\rm O}} \bar{n}_{\rm P}^{\rm O} - \frac{c_{\rm Nb}}{c_{\rm O}} \bar{n}_{\rm Nb}^{\rm O},$$
 (6)

where N_{NBO} is the number of NBO atoms. The fraction of BO atoms is given by $f_{\rm BO}$ = 1 - $f_{\rm NBO}$. If all of the NBO species are associated with phosphorus, the NBO:P ratio is given by $N_{\rm NBO}/N_{\rm P}$ = $c_{\rm O} f_{\rm NBO}/c_{\rm P}$. For $\bar{n}_{\rm P}^{\rm O}$ = 4, the BO:P ratio follows from $N_{\rm BO}/N_{\rm P}$ = $4 - N_{\text{NBO}}/N_{\text{P}}$, where N_{BO} is the number of BO atoms.

The number of P-O-P connections per phosphorus atom is given by

$$\frac{N_{\text{POP}}}{N_{\text{P}}} = 4 - \frac{N_{\text{NBO}}}{N_{\text{P}}} - \frac{N_{\text{PONb}}}{N_{\text{P}}}.$$
 (7)

The oxygen to phosphorus ratio for those O atoms connected to P is given by

$$\frac{N_{\rm O,P}}{N_{\rm P}} = \frac{N_{\rm NBO}}{N_{\rm P}} + \frac{N_{\rm PONb}}{N_{\rm P}} + \frac{N_{\rm POP}}{2N_{\rm P}},$$
 (8)

where the factor of 1/2 in the last term avoids the double counting of BO atoms in P-O-P connections. The O:P ratio for the glass is given by $N_{\rm O}/N_{\rm P} = c_{\rm O}/c_{\rm P}$ but all of the O atoms are not necessarily associated with P atoms because of the possibility of Nb-O-Nb connections. The fraction of oxygen atoms in these connections is given by

$$f_{\text{NbONb}} = \frac{(N_{\text{O}}/N_{\text{P}}) - (N_{\text{O,P}}/N_{\text{P}})}{(N_{\text{O}}/N_{\text{P}})}.$$
 (9)

Let $\kappa = N_{\text{NbOP}}/N_{\text{Nb}}$ denote the mean number of Nb-O-P bonds per Nb atom. The number of Nb-O-P bonds is equal to the number of P-O-Nb bonds, so the number of P-O-Nb bonds per phosphorus atom is given by $N_{PONb}/N_P = c_{Nb}\kappa/c_P$. The parameter κ can be viewed as a measure of the preference for the formation of heteroatomic P-O-Nb linkages over homoatomic Nb-O-Nb and P-O-P linkages. If κ is sufficiently large, then N_{PONb}/N_{P} will increase and N_{POP}/N_P will decrease with increasing x until $N_{\text{POP}}/N_{\text{P}} = 0$ at some value $x_0 < 0.5$. Then, for $x > x_0$, there will no longer be P-O-P bonds to be consumed by Nb, but the remaining P-NBO connections can be replaced by P-O-Nb connections, such

$$\frac{N_{\rm PONb}}{N_{\rm P}}(x \ge x_0) = \frac{N_{\rm PONb}}{N_{\rm P}}(x_0) + \left[\frac{N_{\rm NBO}}{N_{\rm P}}(x_0) - \frac{N_{\rm NBO}}{N_{\rm P}}(x)\right]. \quad (10)$$

At x = 0, this model gives $N_{\text{NBO}}/N_{\text{P}} = 2$, $N_{\text{POP}}/N_{\text{P}} = 2$, and $N_{\text{PONb}}/N_{\text{P}} = 0$ as found for crystalline NaPO₃.³⁰ At x = 0.5with $\bar{n}_{Nb}^{O} = 6$, it gives $N_{NBO}/N_P = 0$, $N_{POP}/N_P = 0$, $N_{PONb}/N_P = 4$, and $f_{\text{NbONb}} = 0.5$, as found for the crystalline polymorphs of Na₄Nb₈P₄O₃₂ with space groups $P2_1^{32}$ and $P2_1/c$.¹⁹ The model with $\bar{n}_{Nb}^{O} = 6$ and $\kappa = 3$ gives $N_{NBO}/N_{P} = 1$, $N_{POP}/N_{P} = 0$, and $f_{\text{NbONb}} = 0.2727$ as found for crystalline CaNb₂P₂O₁₁, which sits at x = 0.5 on the related $(Nb_2O_5)_x(CaP_2O_6)_{1-x}$ pseudo-binary

The model leading to Eq. (10) assumes that the addition of Nb leads to the preferential formation of P-O-Nb bonds, such that all the P-O-P bonds are consumed at a composition $x_0 < 0.5$. To provide a reference point, it is instructive to consider how the predictions compare to those obtained from an alternative model in which there is a statistical distribution of P-O-P, P-O-Nb and Nb-O-Nb linkages.42

The number of P-O-Nb linkages per phosphorus atom $N_{\rm PONb}/N_{\rm P}$ can be found by first considering a binomial distribution of P-BO and P-NBO bonds, such that the fraction of Pⁿ species with *n* P-O-P plus P-O-Nb bonds is given by

$$f_{P^n} = \frac{4!}{n!(4-n)!} (1-p_{\text{PNBO}})^n p_{\text{PNBO}}^{(4-n)}, \tag{11}$$

where the probability of a P-NBO linkage is given by $p_{\text{PNBO}} = N_{\text{PNBO}}/N_{\text{PO}}$, $N_{\text{PNBO}} = N_{\text{NBO}}$ is the number of P-NBO bonds found from Eq. (6), and $N_{PO} = N_P \bar{n}_P^O$ is the total number of P-O bonds. Equation (11) distributes the NBO atoms among the phosphorus sites but does not alter the composition dependence of $N_{\rm NBO}/N_{\rm P}$. The fraction of Pⁿ species that form m P-O-Nb bonds $(m \le n)$ can then be found by considering a binomial distribution of P-O-Nb and P-O-P bonds, such that the fraction of P_{mNb}^n species

$$f_{P_{mNb}^n} = \frac{n!}{m!(n-m)!} p_{PONb}^m (1 - p_{PONb})^{(n-m)},$$
 (12)

where the probability of a P-O-Nb linkage is given by $p_{\text{PONb}} = N_{\text{NbO}}/(N_{\text{PBO}} + N_{\text{NbO}}), N_{\text{NbO}} = N_{\text{Nb}}\bar{n}_{\text{Nb}}^{\text{O}}$ is the number of Nb-O bonds, $N_{\text{PBO}} = N_{\text{P}} \bar{n}_{\text{P}}^{\text{BO}}$ is the number of P-BO bonds, and $\bar{n}_{\rm P}^{\rm BO}$ = 4 – $N_{\rm NBO}/N_{\rm P}$. The probability of a P–O–P linkage is given by $1 - p_{PONb}$. The N_{PONb}/N_P and N_{POP}/N_P ratios can be found from the calculated P_{mNb}^n speciation. The fraction of oxygen atoms in Nb-O-Nb connections follows from Eq. (9).

An alternative method for obtaining the statistical distribution of P-O-P, P-O-Nb, and Nb-O-Nb linkages is to consider the probability of finding a P-O-P linkage, which is proportional to the weighting factor,

$$W_{\text{POP}} = \left(c_{\text{P}}\bar{n}_{\text{P}}^{\text{BO}}\right)^2/2,\tag{13}$$

the probability of finding an Nb-O-Nb linkage, which is proportional to the weighting factor,

$$W_{\text{NbONb}} = \left(c_{\text{Nb}}\bar{n}_{\text{Nb}}^{\text{BO}}\right)^2/2,$$
 (14)

and the probability of finding a P-O-Nb linkage, which is proportional to the weighting factor,

$$W_{\text{PONb}} = c_{\text{P}} \bar{n}_{\text{P}}^{\text{BO}} c_{\text{Nb}} \bar{n}_{\text{Nb}}^{\text{BO}}. \tag{15}$$

The factor of 1/2 in Eqs. (13) and (14) avoids the double counting of P-O-P or Nb-O-Nb connections. The associated probabilities of finding a BO atom in a P-O-P, Nb-O-Nb, or P-O-Nb connection are given by $P_{POP} = N_{O, POP}/N_{BO} = W_{POP}/(W_{POP} + W_{NbONb})$ + W_{PONb}), $P_{NbONb} = N_{O, NbONb}/N_{BO} = W_{NbONb}/(W_{POP} + W_{NbONb})$ + W_{PONb}), and $P_{PONb} = N_{O,PONb}/N_{BO} = W_{PONb}/(W_{POP} + W_{NbONb})$ + W_{PONb}), respectively, where $N_{\text{O, POP}}$, $N_{\text{O, NbONb}}$, and $N_{\text{O, PONb}}$ are the numbers of BO atoms in these connections, respectively. The composition dependence of the probabilities is shown in Fig. 8 for the case when $\bar{n}_{\rm Nb}^{\rm BO}=\bar{n}_{\rm Nb}^{\rm O}=6$.

The number of P-O-P connections per P atom is given by

$$\frac{N_{\rm POP}}{N_{\rm P}} = \frac{2N_{\rm O,POP}}{N_{\rm BO}} \frac{N_{\rm BO}}{N_{\rm O}} \frac{N_{\rm O}}{N} \frac{N}{N_{\rm P}} = 2P_{\rm POP} f_{\rm BO} \frac{c_{\rm O}}{c_{\rm P}}. \tag{16}$$

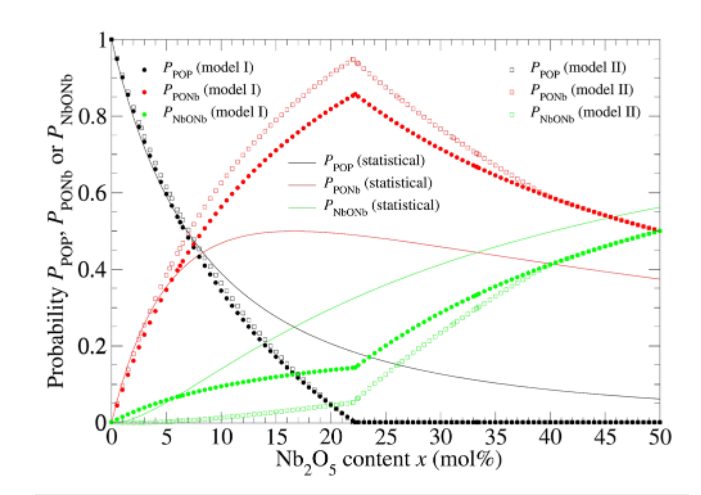


FIG. 8. Composition dependence of the probabilities P_{POP} , P_{NbONb} , and P_{PONb} of finding a BO atom in a P-O-P, Nb-O-Nb, or P-O-Nb connection, respectively, for $\bar{n}_{Nb}^{O}=6$. The solid circles represent the results of model I (Sec. V A) with $\kappa=4.5$; the open squares represent the results of model II (Sec. V D) with $\kappa = 5$; and the solid curves represent the results obtained by assuming a statistical distribution of these connections.

The number of P-O-Nb connections per P atom is given by

$$\frac{N_{\rm PONb}}{N_{\rm P}} = \frac{N_{\rm O,PONb}}{N_{\rm BO}} \frac{N_{\rm BO}}{N_{\rm O}} \frac{N_{\rm O}}{N} \frac{N}{N_{\rm P}} = P_{\rm PONb} f_{\rm BO} \frac{c_{\rm O}}{c_{\rm P}}. \tag{17}$$

The number of NBO atoms per P atom $N_{\rm NBO}/N_{\rm P}$ then follows from Eq. (7). The oxygen to phosphorus ratio for those O atoms connected to P is given by Eq. (8), and the fraction of oxygen atoms in Nb-O-Nb connections is given by Eq. (9). Both methods for calculating the statistical distribution of linkages are consistent with one another, with the first providing access to the fractions $f_{P_{mNh}^n}$

A statistical distribution of P-O-P, P-O-Nb, and Nb-O-Nb linkages with $\bar{n}_{\text{Nb}}^{\text{O}} = 6$ gives the expected ratio $N_{\text{PONb}}/N_{\text{POP}} = 2$ at the composition x = 1/3, where $N_{\rm NBO}/N_{\rm P} = 1$ and the Nb:P ratio is 1:1. It also gives $N_{PONb}/N_{POP} = 3$ at x = 0.5 where $N_{NBO}/N_{P} = 0$ and the Nb:P ratio is 2:1. In contrast, P-O-P bonds are absent in the model crystalline compound Na₄Nb₈P₄O₃₂, ^{19,32} which corresponds to the x = 0.5 composition; i.e., this crystal structure does not correspond to a statistical distribution of P-O-P, P-O-Nb, and Nb-O-Nb linkages.

B. Comparison between the models and experiment

Figure 9 shows that model I of Sec. V A with $\bar{n}_{\rm P}^{\rm O} = 4$ and $\bar{n}_{\rm Nb}^{\rm O} = 6$ gives a good account of the $N_{\rm NBO}/N_{\rm P}$ values found in our ³¹P solidstate NMR work¹² (Table III). If $\kappa \simeq 4.5$, the model also provides a good account of the composition dependence of the measured $N_{\text{PONb}}/N_{\text{P}}$, $N_{\text{POP}}/N_{\text{P}}$, and f_{NbONb} values (Figs. 10-12). Here, the increase in the number of negatively charged [NbØ_{6/2}] motifs with increasing x will require a reduction in the P:NBO ratio. According to the crystal structures along the Nb₂O₅-NaPO₃ pseudo-binary tie-line, the $[P\emptyset_{2/2}O_2]^-$ groups at x = 0 will be replaced by $[P\emptyset_{4/2}]^+$ For the latter, the Nb:Na:P ratio is 2:1:1, such that the combined charge on an Na⁺ ion and phosphate group is balanced by the charge on two $[Nb\emptyset_{6/2}]^-$ motifs.

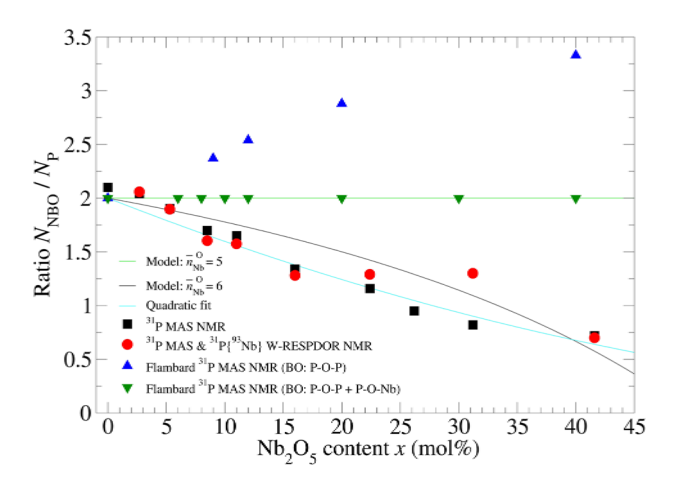


FIG. 9. Composition dependence of the ratio $N_{\rm NBO}/N_{\rm P}$. The symbols correspond to the ³¹P NMR results from the work of Ensuncho et al. ¹² and Flambard et al. In the former work, $N_{\rm NBO}/N_{\rm P}$ was found either directly from the $P_{m{\rm Nb}}^n$ speciation (Table III) or from Eq. (7) with N_{POP}/N_P taken from the ^{31}P MAS NMR results and $N_{\text{PONb}}/N_{\text{P}}$ taken from the ³¹P(⁹³Nb) W-RESPDOR NMR results. In the latter work, the BO atoms were considered to be in either P-O-P or both P-O-P and P-O-Nb connections. The green and black curves are from Eq. (6) of model I with $\bar{n}_{p}^{0} = 4$ and an \bar{n}_{Nb}^{O} value of either 5 or 6, respectively. The cyan curve represents a parabolic fit to the ³¹P MAS NMR results of Ensuncho et al. ¹²

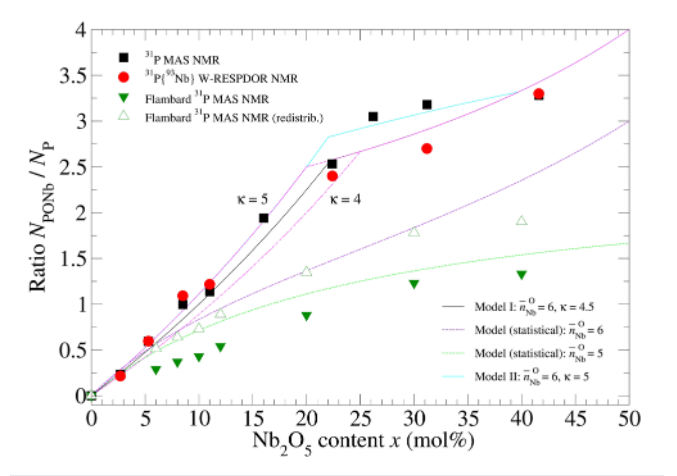


FIG. 10. Composition dependence of the ratio $N_{\rm PONb}/N_{\rm P}$. As in Fig. 9, the symbols correspond to the NMR results of Ensuncho *et al.* 12 and Flambard *et al.* 4 In the latter work, the number of P=O bonds was either kept at the value found from the measured phosphorus speciation or the P=O bonds were redistributed to P-O-Nb and P–O–Na connections, thereby increasing their numbers (Sec. V E). The black curve is from model I with $\bar{n}_{Nb}^{O}=6$ and $\kappa=4.5$. The magenta chained and broken curves correspond to model I with $\bar{n}_{Nb}^{O}=6$ and either $\kappa=4$ or $\kappa=5$, respectively. The violet and green broken curves are from the model for a statistical distribution of P-O-P, P-O-Nb, and Nb-O-Nb linkages with an $\bar{n}_{\rm Nb}^{\rm O}$ value of either 6 or 5, respectively. The cyan curve is from model II with $\bar{n}_{Nb}^{O}=6$ and $\kappa=5$.

In contrast to the experiment, a statistical distribution of P-O-Nb, P-O-P, and Nb-O-Nb linkages, with $N_{\rm NBO}/N_{\rm P}$ calculated from Eq. (6) by assuming that \bar{n}_{Nb}^{O} takes the value of 6 or 5, does not lead to the elimination of P-O-P bonds with increasing

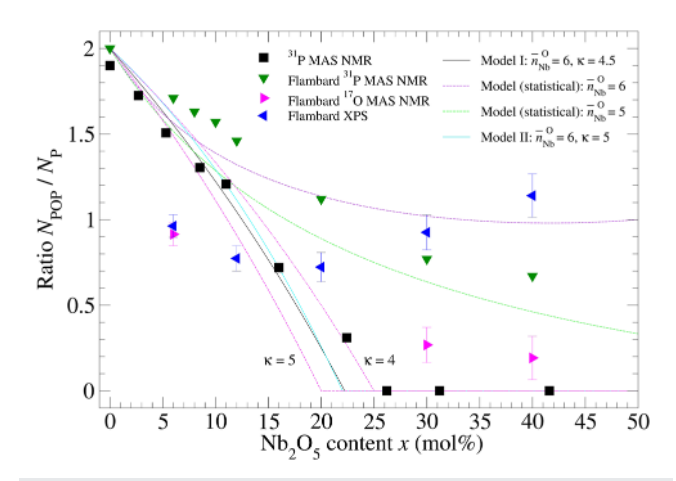


FIG. 11. Composition dependence of the ratio $N_{\text{POP}}/N_{\text{P}}$. The symbols correspond to the 31 P MAS NMR results of Ensuncho *et al.* ¹² and to the 31 P and 17 O MAS NMR and XPS results of Flambard *et al.* ⁴ The black curve is from model I with $\bar{n}_{\text{Nb}}^{0}=6$ and $\kappa=4.5$. The magenta chained and broken curves correspond to model I with $\bar{n}_{\text{Nb}}^{0}=6$ and either $\kappa=4$ or $\kappa=5$, respectively. The violet and green broken curves are from the model for a statistical distribution of P–O–P, P–O–Nb, and Nb–O–Nb linkages with an \bar{n}_{Nb}^{0} value of either 6 or 5, respectively. The cyan curve is from model II with $\bar{n}_{\text{Nb}}^{0}=6$ and $\kappa=5$.

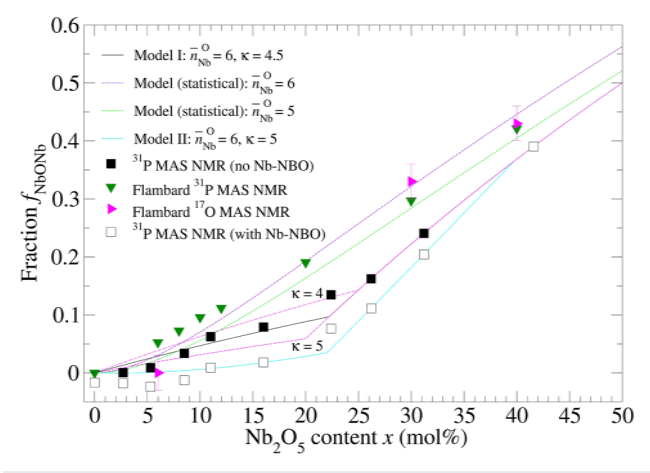


FIG. 12. Composition dependence of the fraction f_{NbONb} . The symbols correspond to the NMR results of Ensuncho *et al.*¹² and Flambard *et al.*⁴ In the former work, either Eq. (9) (no Nb-NBO connections) or Eq. (21) (Nb–O connections allowed) was used with $N_{\text{O,P}}/N_{\text{P}}$ calculated from the 31 P MAS NMR results using Eq. (8). The black curve is from model I with $\bar{n}_{\text{Nb}}^{O} = 6$ and $\kappa = 4.5$. The magenta chained and broken curves correspond to model I with $\bar{n}_{\text{Nb}}^{O} = 6$ and $\kappa = 4$ or $\kappa = 5$, respectively. The violet and green broken curves are from the model for a statistical distribution of P–O–P, P–O–Nb, and Nb–O–Nb linkages with an \bar{n}_{Nb}^{O} value of either 6 or 5, respectively. The cyan curve is from model II with $\bar{n}_{\text{Nb}}^{O} = 6$ and $\kappa = 5$.

x (Fig. 11). The slower decrease in $N_{\rm POP}/N_{\rm P}$ with increasing x leads, at a given composition, to fewer P–O–Nb bonds (Fig. 10) and a concomitant higher fraction of oxygen atoms in Nb–O–Nb connections (Fig. 12).

The Raman spectra (Sec. IV D) are in-line with the solid-state NMR results. As the niobia content first increases, the spectra

indicate the elimination of P–O–P connections. As the niobia content increases beyond x=0.05, they are also compatible with the NbO₆ units making fewer Nb–O–P and more Nb–O–Nb connections. The findings are in qualitative accord with the expectations of the probabilities P_{POP} , P_{PONb} , and P_{NbONb} for the model with $\kappa=4.5$ (Fig. 8). It is notable that in the reported crystal structures for Na₄Nb₈P₄O₃₂, ^{19,32} which correspond to the x=0.5 composition, each PO₄ unit makes 4 P–O–Nb connections such that P–O–P connections are absent.

C. Next nearest-neighbor O-O correlations

In the glass, the shortest O–O distances at $\simeq 2.52$ Å originate from the oxygen atoms within or between the phosphate groups. The associated coordination number $\tilde{n}_{\rm O}^{\rm O}({\rm short})$ can be calculated accordingly (Sec. IV C). The next nearest-neighbor O–O distances at $\simeq 2.80$ –2.83 Å will originate from the shorter O–O distances associated with the distorted NbO₆ polyhedral units of the framework structure in which the Na⁺ ions reside (see the discussion at the start of Sec. V). The associated O–O coordination number is given by

$$\tilde{n}_{O}^{O}(\log) = \frac{1}{N_{O}} \left(N_{O,NbONb} \tilde{n}_{O,NbONb}^{O} + N_{O,PONb} \tilde{n}_{O,PONb}^{O} \right)
= \frac{N_{NbONb}}{N_{O}} \tilde{n}_{O,NbONb}^{O} + \frac{N_{PONb}}{N_{P}} \frac{N_{P}}{N_{O}} \tilde{n}_{O,PONb}^{O}
= f_{NbONb} \tilde{n}_{O,NbONb}^{O} + \frac{N_{PONb}}{N_{P}} \frac{c_{P}}{c_{O}} \tilde{n}_{O,PONb}^{O},$$
(18)

where $N_{\rm O,NbONb}$ is the number of oxygen atoms in Nb–O–Nb linkages, and $\bar{n}_{\rm O,NbONb}^{\rm O}$ and $\bar{n}_{\rm O,PONb}^{\rm O}$ are the coordination numbers for the oxygen atoms in Nb–O–Nb and P–O–Nb linkages, respectively, for O–O distances of \simeq 2.80–2.83 Å. The number of Nb–O–Nb linkages is given by $N_{\rm NbONb} = N_{\rm O,NbONb}$, and the fraction of oxygen atoms in Nb–O–Nb linkages is given by $f_{\rm NbONb} = N_{\rm NbONb}/N_{\rm O}$. The $f_{\rm NbONb}$ and $N_{\rm PONb}/N_{\rm P}$ parameters can be found from the $^{31}{\rm P}$ MAS NMR results (Sec. V A).

In crystalline NbOPO₄, the 1 + 4 + 1 distortion of the NbO₆ octahedron (Table II) leads to oxygen atoms in the P–O–Nb connections with three nearest-neighbor oxygen atoms at 2.495(26) Å, 4 next nearest-neighbor oxygen atoms at 2.790(47) Å, and 2 further oxygen atoms at 2.977 Å, i.e., $\bar{n}_{\text{O,PONb}}^{\text{O}}$ = 4 for an O–O distance of 2.79 Å.²⁷ The oxygen atoms in Nb–O–Nb connections have 4 nearest-neighbor oxygen atoms at 2.806 Å, 4 next nearest-neighbor oxygen atoms at 2.850 Å, and 4 further oxygen atoms at 3.304 Å, i.e., $\bar{n}_{\text{O,NbONb}}^{\text{O}}$ = 4 for an O–O distance of 2.81 Å, which increases to $\bar{n}_{\text{O,NbONb}}^{\text{O}}$ = 8 if the O–O neighbors at 2.85 Å are also included.

For the glasses with x values of 0.1, 0.2, and 0.4, the $\bar{n}_{\rm O}^{\rm O}(\log)$ values calculated from Eq. (18), with $f_{\rm NbONb}$ and $N_{\rm PONb}/N_{\rm P}$ derived from the $^{31}{\rm P}$ MAS NMR results (Table III), are (i) 1.47, 2.76, and 3.51, respectively, if $\bar{n}_{\rm O,PONb}^{\rm O}=\bar{n}_{\rm O,NbONb}^{\rm O}=4$, or (ii) 1.72, 3.30, and 5.07, respectively, if $\bar{n}_{\rm O,PONb}^{\rm O}=4$ and $\bar{n}_{\rm O,NbONb}^{\rm O}=8$. In comparison, the measured $\bar{n}_{\rm O}^{\rm O}(\log)$ values obtained from the peak in $D_{\rm X}'(r)$ at \simeq 2.82 Å are 2.49(15), 3.32(15), and 4.48(15), respectively (Table IV). The findings are consistent with distorted NbO₆ units providing a coordination number $\bar{n}_{\rm O,NbONb}^{\rm O}$ of 6.5–8 for the glasses with $x \geq 0.20$. The large measured value of $\bar{n}_{\rm O}^{\rm O}(\log)$ for the x = 0.10 glass may originate from uncertainty regarding the pair-correlations that contribute toward the peak in $D_{\rm X}'(r)$ at \simeq 2.82 Å [Fig. 6(b)]. There

is probably overlap of the fitted O-O and Na-O contributions with a contribution from the nearest-neighbor P-P distances in cornersharing PO₄ configurations, which occur at 2.870 and 2.967 Å in the crystalline metaphosphate NaPO₃.3

D. Analytical model II for the glass structure: Nb-NBO connections

In analytical model I of Sec. V A, it is assumed that all of the NBO species are associated with the phosphate groups. Figure 9 shows, however, that the predicted $N_{\rm NBO}/N_{\rm P}$ ratio is larger than the measured ratio for several glass compositions, indicting a need to consider the reallocation of a proportion of the NBO species. Indeed, the measured phosphate speciation (Table III) does not, in general, provide sufficient negative charge to balance the positive charge on the Na⁺ ions if all of the niobium atoms are deemed to form [NbØ_{6/2}]⁻ motifs (see Sec. S3). It is, therefore, necessary to consider the possibility of Nb-NBO bonds, which were proposed by Hoppe *et al.*³¹ in their work on the $(Nb_2O_5)_x(NaPO_3)_{1-x}$ system.

The excess in the predicted ratio $(N_{\rm NBO}/N_{\rm P})_{\rm model\,I}$ from model I over the measured ratio $(N_{\rm NBO}/N_{\rm P})_{\rm 31PNMR}$ from the ³¹P MAS NMR experiments can be expressed as

$$\left(\frac{N_{\rm NBO}}{N_{\rm P}}\right)_{\rm ex} = \left(\frac{N_{\rm NBO}}{N_{\rm P}}\right)_{\rm model\,I} - \left(\frac{N_{\rm NBO}}{N_{\rm P}}\right)_{\rm 31PNMR},\tag{19}$$

such that the $N_{\rm NBO}/N_{\rm Nb}$ ratio is given by

$$\frac{N_{\rm NBO}}{N_{\rm Nb}} = \frac{N_{\rm P}}{N_{\rm Nb}} \left(\frac{N_{\rm NBO}}{N_{\rm P}}\right)_{\rm ex} = \frac{c_{\rm P}}{c_{\rm Nb}} \left(\frac{N_{\rm NBO}}{N_{\rm P}}\right)_{\rm ex}. \tag{20}$$

The resultant reduction in $N_{\rm NBO}/N_{\rm P}$ has a concomitant effect on the $N_{\rm POP}/N_{\rm P}$ and $N_{\rm PONb}/N_{\rm P}$ ratios via Eq. (7). There is also an alteration to the number of BO atoms involved in Nb-O-Nb connections because a fraction of the oxygen atoms bound to Nb are now NBO species. Equation (9) becomes

$$f_{\text{NbONb}} = \frac{(N_{\text{O}}/N_{\text{P}}) - (N_{\text{O,P}}/N_{\text{P}}) - (N_{\text{NBO}}/N_{\text{P}})_{\text{ex}}}{(N_{\text{O}}/N_{\text{P}})}.$$
 (21)

Figure 9 shows the effect of fitting a quadratic approximation to the composition dependence of the ³¹P MAS NMR results for $N_{\rm NBO}/N_{\rm P}$ to find $(N_{\rm NBO}/N_{\rm P})_{31\rm PNMR}$ for use in Eq. (19). The associated reassignment of NBO atoms from P to Nb atoms via Eq. (20) results in a composition dependence of $N_{\rm PONb}/N_{\rm P}$ that can be represented by choosing $\kappa = 5$ (Fig. 10). The composition dependencies of N_{POP}/N_P and f_{NbONb} are shown in Figs. 11 and 12, respectively. Relative to model I with $\kappa = 4.5$, there is little change to N_{POP}/N_P but a decrease in the fraction of BO atoms in Nb-O-Nb linkages.

As discussed in Sec. S3, Fig. S2 compares the composition dependence of the $N_{\rm NBO}/N_{\rm Nb}$ ratio found from model II with the expectations from three different scenarios for interpreting the composition dependence of the experimental results. The model indicates that $N_{\rm NBO}/N_{\rm Nb}=1$ at $x\simeq 0.04$, such that all of the Nb atoms are in $[{\rm Nb}\varnothing_{5/2}{\rm O}]^{2-}$ units. The predictions of the model are in overall agreement with the experimental findings for x > 0.075, showing that the fraction of NBO atoms in the Nb-centered units decreases monotonically with increasing x and vanishes near x = 0.40such that all of the Nb atoms are in $[Nb\emptyset_{6/2}]^-$ units. This behavior is consistent with the structure of crystalline Na₄Nb₈P₄O₃₂

(x = 0.5) in which Nb-NBO bonds are absent. For $x \le 0.075$, the $N_{
m NBO}/N_{
m Nb}$ values are more uncertain. As discussed in Sec. S3, the scenario providing the most reasonable account of the experimental results across the entire composition range suggests that the number of NBO atoms per Nb-centered units diminishes to zero as the Nb_2O_5 content decreases from x = 0.075.

As shown in Fig. 8, model II with $\kappa = 5$ has little effect on the probability of finding a BO atom in a P-O-P connection, which is set by the findings from the ³¹P MAS NMR experiments. Relative to model I with κ = 4.5, there is an increased probability of finding a BO atom in a P-O-Nb connection and a decreased probability of finding a BO atom in a Nb-O-Nb connection as the Nb₂O₅ content of the glass increases to $x \simeq 0.4$. At larger x-values, $(N_{\text{NBO}}/N_{\text{P}})_{\text{ex}} = 0$, such that $N_{\text{NBO}}/N_{\text{Nb}} = 0$ and these probabilities are calculated using model I with $\kappa = 5$.

E. Comparison with previous work

The P^n speciation, where *n* refers to the number of BO atoms in P-O-P connections alone, is reported in the ³¹P MAS NMR work of Flambard et al.^{3,4} The associated $N_{\rm NBO}/N_{\rm P}$ values can be found by assuming that the remaining connections in a phosphate group are P-NBO bonds. These $N_{\rm BO}/N_{\rm P}$ and $N_{\rm NBO}/N_{\rm P}$ values were used by Hoppe et al.³¹ in the analysis of their diffraction data. Alternatively, other bonds can be included in the distribution of the remaining connections. Flambard et al.4 assumed a model that is equivalent to each P atom making n P-O-P bonds, 1 P=O double bond, and 1 P-O-Na bond, such that the number of P-O-Nb bonds per phosphorus atom is given by $N_{PONb}/N_P = 4 - 2 - n = 2 - n$. In this model, $N_{\text{NBO}}/N_{\text{P}} = 2$ across the composition range if all of the oxygen atoms in P=O and P-O-Na connections are regarded as NBO atoms (Fig. 9). This $N_{\rm NBO}/N_{\rm P}=2$ finding is reproduced by Eq. (6) with $\bar{n}_{P}^{O} = 4$ and $\bar{n}_{Nb}^{O} = 5$ (Fig. 9). At each composition, the P:Na ratio is 1:1 and the negative charge on the network structure that is required to balance the positive charge on the Na⁺ ions is provided by the $[P\emptyset_{2/2}O_2]^-$ phosphate groups alone, thus requiring charge neutral $[Nb\emptyset_{5/2}]^0$ species. In consequence, the model of Flambard et al.4 is inconsistent with the notion of six-coordinated Nb atoms, as suggested by their 93Nb MAS NMR and Raman spectroscopy results.

In the work of Flambard et al.,4 there is also significant discrepancy in the composition dependence of $N_{\rm POP}/N_{\rm P}$ as deduced from their ³¹P MAS NMR, ¹⁷O MAS NMR, and x-ray photoelectron spectroscopy (XPS) experiments (Fig. 11). In a further step during the analysis of their ³¹P MAS NMR spectra, an allowance was made for the delocalization of the P=O bonds via a procedure in which these bonds were redistributed to form additional P-O-Na and P-O-Nb connections in proportion to the modeled $N_{PONa}/N_{PO(Na,Nb)}$ and $N_{\rm PONb}/N_{\rm PO(Na,Nb)}$ ratios, respectively. This redistribution has no effect on N_{POP}/N_P or f_{NbONb} , where the values of the latter are in accordance with those deduced from the ¹⁷O MAS NMR experiments (Fig. 12). It leads, however, to increases in N_{PONb}/N_{P} (Fig. 10) and N_{PONa}/N_P relative to the case when no redistribution is made.

The statistical distribution of P-O-P, P-O-Nb, and Nb-O-Nb linkages, with $N_{\rm NBO}/N_{\rm P}$ calculated from Eq. (6) and $\bar{n}_{\rm Nb}^{\rm O}$ = 6, gives a good account of the composition dependence of the Flambard et al.⁴ results for f_{NbONb} (Fig. 12) and for N_{PONb}/N_P after the P=O bonds are redistributed (Fig. 10). A coordination number $\bar{n}_{Nb}^{O} = 5$ is, however, necessary to reproduce the assumed value of $N_{\rm NBO}/N_{\rm P}=2$ across the composition range (Fig. 9).

In summary, Figs. 9-12 show clear contrast between the findings of the present work and those obtained from either of the models of Flambard et al.3,4 In particular, the new experimental results show an elimination of the P–O–P connections at $x_0 \sim 0.22$. A self-consistent account of the composition dependence of all the newly measured parameters is provided by models I and II, which incorporate four- and six-coordinated P and Nb atoms, respectively, along with the preferential formation of P-O-Nb bonds as the niobia content of the glass increases. The P-O and Nb-O coordination numbers of 4 and 6, respectively, are supported by the present findings from the diffraction, solid-state NMR, and Raman spectroscopy experiments. The results, therefore, call for a reinterpretation of the measured ¹⁷O MAS NMR and XPS spectra for these materials.³

F. Structure-property relationships

1. Class transition temperature

Figures 9-12 show that the connectivity of the P and Nb centered network forming motifs changes substantially with the niobium oxide content of the glass. The density of the P-O-P, P-O-Nb, and Nb-O-Nb connections between these motifs can be calculated from the expression,

$$\rho_{\rm con} = \rho_0 \left(\frac{c_{\rm P}}{2} \frac{N_{\rm POP}}{N_{\rm P}} + c_{\rm P} \frac{N_{\rm PONb}}{N_{\rm P}} + c_{\rm O} f_{\rm NbONb} \right), \tag{22}$$

where $\rho_0 = N/V$ is the number density, V is the volume, and the factor of 1/2 in the first term avoids the double counting of P-O-P connections. The connectivity density for the $(Nb_2O_5)_x(NaPO_3)_{1-x}$ glasses was calculated from model I of Sec. V A using the mean value $\rho_0 = 0.0728 \text{ Å}^{-3}$: the number density changes by only ~2.5% across the composition range. Figure 1(b) shows that $\rho_{\rm con}$ and $T_{\rm g}$ share almost exactly the same composition dependence, which supports the notion of the Nb⁵⁺ ions taking a network forming role. Model II with $\kappa = 5$ reassigns a fraction of the NBO atoms from the P to the Nb atoms but does not alter the fraction of BO connections, i.e., the connectivity density $\rho_{\rm con}$ is not altered.

2. Non-linear optical properties

For the $(Nb_2O_5)_x(NaPO_3)_{1-x}$ system, a large increase in the non-linear optical index n2 with the Nb2O5 content of the glass is reported for x > 0.2. Models I and II both show an increase to the rate-of-change of f_{NbONb} with x, beyond the $x_0 \sim 0.22$ limit (Fig. 12) at which the P-O-P connections are eliminated (Fig. 11). The findings support the notion that the increase in n_2 for x > 0.2 is associated with the formation of larger clusters of octahedral NbO₆ units that involve highly polarizable Nb-O-Nb connections.⁴

3. Chemical durability

structure and properties of glasses in $(Nb_2O_5)_x(Na_2O)_{0.4}(P_2O_5)_{0.6-x}$ series $(0 \le x \le 0.40)$ have been investigated by Mošner et al.⁸ and others.⁴³ The glass with x = 0.20matches the (Nb₂O₅)_{0.20}(NaPO₃)_{0.80} composition investigated in the present work. Figure 13 shows that the measured density, glass transition temperature, and dissolution rate all display a change in behavior at $x \sim 0.3$. A decrease in the proportion of P-O-P

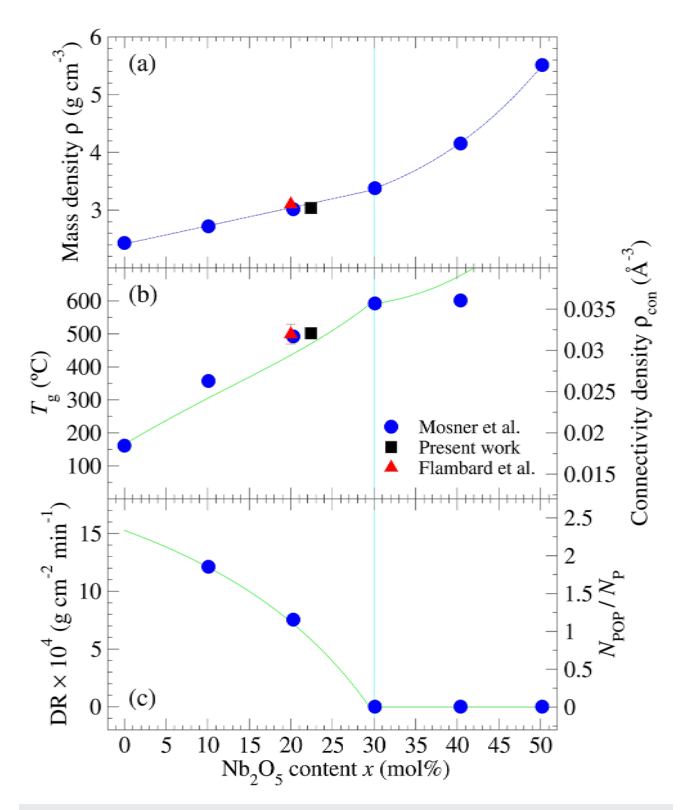


FIG. 13. Composition dependence of (a) the mass density ρ , (b) the glass transition temperature T_g , and (c) the dissolution rate (DR) found in the work of Mošner $et~al.^8$ for the (Nb₂O₅)_x(Na₂O)_{0.4}(P₂O₅)_{0.6-x} glass series. In panels (a) and (b), the ρ and T_g values at $x\simeq 20$ mol. % from the present work and Flambard $et~al.^4$ are also provided. In panel (a), the blue broken curve is drawn as a guide for the eye. In panels (b) and (c), the green curves represent the composition dependence of the connectivity density and the $N_{\text{POP}}/N_{\text{P}}$ ratio, respectively, as calculated from model I with $\kappa = 2.75$. The cyan vertical line marks the x = 30 mol. % composition.

bonds with increasing x was inferred from ³¹P MAS NMR spectra,⁸ although a quantitative analysis of the phosphorus speciation was not performed. In the absence of this information, it is not possible to deduce the $N_{\rm NBO}/N_{\rm Nb}$ ratio. Model I of Sec. V A was, therefore, used to interpret the results.

Figure S3 shows that model I predicts a progressive removal of P–O–P connections with increasing *x* and leads to their elimination at $x_0 \sim 0.3$ when $\kappa \sim 2.5-3$. Figure 13(b) shows that the composition dependence of $\rho_{\rm con}$, as calculated using $\kappa = 2.75$ and ρ_0 values found from the measured mass density [Fig. 13(a)], matches the composition dependence of T_g , showing a change in slope at $x_0 \sim 0.3$. Figure 13(c) shows that the composition dependence of N_{POP}/N_P found from the model matches almost exactly the measured composition dependence of the dissolution rate. The findings indicate that the observed changes to the material properties are related to the consumption of P-O-P bonds as the niobia content of the glass is increased, suggesting that the P-O-P connections provide hydrolysis pathways. The dissolution rate is zero, and the chemical durability is enhanced when P-O-P bonds are absent from the glass structure.

Figure S4 shows the effect of setting $\kappa = 4$ on the predictions of model I for the connectivity density and the N_{POP}/N_P ratio for

the $(Nb_2O_5)_x(Na_2O)_{0.4}(P_2O_5)_{0.6-x}$ glass series. This κ value better represents the results found from the 31P MAS NMR study of the glass with nominal composition $(Nb_2O_5)_{0.20}(NaPO_3)_{0.80}$, which matches the composition of the $(Nb_2O_5)_x(Na_2O)_{0.4}(P_2O_5)_{0.6-x}$ glass with x = 0.20. The change in the κ value does not, however, alter the premise that the dissolution rate is affected by the fraction of P-O-P bonds present in the glass structure, nor the finding that the connectivity density can account for the main features in the composition dependence of T_g , which supports a network forming role for Nb_2O_5 .

VI. CONCLUSIONS

The structure of $(Nb_2O_5)_x(NaPO_3)_{1-x}$ glasses was investigated by neutron and x-ray diffraction and Raman scattering, supported by the results obtained from conventional and advanced solid state NMR spectroscopy. 12 The Nb-centered motifs are found to adopt a distorted octahedral coordination environment at all of the glass compositions. Along with the phosphate groups, they contribute toward a network structure that shows a significant evolution with increasing niobia content. The findings contrast to those found previously,^{3,4} revealing a significant reduction in the fraction of P–O–P linkages with increasing x, which leads to the elimination of these connections at a composition $x_0 \sim 0.22$, and a preferential formation of P-O-Nb linkages. The results indicate that Nb acts as a network former in this glass system. At low x-values, P^2 species predominate, with a fraction of them forming P-O-Nb linkages, and Nb-O-Nb connections may also be created. As x increases beyond x_0 , P_{3Nb}^3 species are found to predominate and P_{4Nb}^4 species begin to form as the fraction of Nb-O-Nb connections increases more rapidly.

Two analytical models were developed in which a network structure is created from 4-coordinated P and 6-coordinated Nb atoms, and there is a preferential formation of P-O-Nb bonds when niobium is introduced such that P-O-P connections are absent when the niobia content exceeds x_0 . In model II, Nb-NBO bonds are invoked to ensure overall charge neutrality and Nb–O–Nb linkages are only formed at x > 0.10. In contrast to previous work,4 the models provide a self-consistent account of the composition dependence of all the measured parameters for both the glassy and crystalline materials along the Nb₂O₅-NaPO₃ pseudobinary tie-line. This account includes crystalline Na₄Nb₈P₄O₃₂, ¹⁹ which marks the limit of the glass-forming region near x = 0.5, and has a structure based entirely on P4_{Nb} network forming

The models deliver a composition-dependent connectivity density $\rho_{\rm con}$ that matches the trend of the glass transition temperature, thus confirming a network-forming role for the Nb atoms. The rapid increase in the non-linear optical properties reported for $x > 0.2^4$ coincides with an increase in the rate-of-change of $f_{\rm NbONb}$ with x beyond $x_0 \sim 0.22$, i.e., it is related to a more rapid increase in the fraction of oxygen atoms involved in polarizable Nb-O-Nb connections. The application of model I to glasses in the $(Nb_2O_5)_x(Na_2O)_{0.4}(P_2O_5)_{0.6-x}$ series indicates that changes to $T_{\rm g}$ and the dissolution rate are related to the elimination of P–O–P bonds with increasing niobia content. The modeling approach, therefore, offers insight into designing phosphate glass structures with the desired physico-chemical properties.

SUPPLEMENTAL MATERIAL

Section S2 of the supplementary material provides the composition dependence of the molar volume $V_{\rm mol}$ per atom and per oxygen atom for the $(Nb_2O_5)_x(NaPO_3)_{1-x}$ glass series. Section S3 describes the effect in model II of transferring NBO atoms from P to Nb atoms and quantifies the composition dependence of $N_{\rm NBO}/N_{\rm Nb}$, comparing the results with those found from experiment according to three different scenarios for determining the exact glass compositions. In Sec. S3, the composition dependence of $N_{\text{NBO}}/N_{\text{P}}$, $N_{\text{POP}}/N_{\text{P}}$, $N_{\text{PONb}}/N_{\text{P}}$, and f_{NbONb} is calculated for the $(Nb_2O_5)_x(Na_2O)_{0.4}(P_2O_5)_{0.6-x}$ glass series using $\bar{n}_{Nb}^O=6$ and either (i) model I of Sec. V A for different κ values or (ii) a statistical distribution of P-O-P, P-O-Nb, and Nb-O-Nb connections. For the $(Nb_2O_5)_x(Na_2O)_{0.4}(P_2O_5)_{0.6-x}$ glass series, the effect of changing from the value κ = 2.75 to the value κ = 4 on the predictions of model I for both the connectivity density and the N_{POP}/N_P ratio is discussed.

ACKNOWLEDGMENTS

We thank Gavin Vaughan (ESRF) for help with the ID15A experiments, Hesameddin Mohammadi (Bath) for measuring the glass and crystal densities by He pycnometry, and Alain Bertoni (ILL) for help with the D4c experiments. We appreciate the support received via the FAPESP/Bath University SPRINT Programme, Process No. 2022/14232-0 and the support by FAPESP via the Center for Research, Technology, and Education in Vitreous Materials (CeRTEV), Process No. 2013/07793-6. E.G.L. acknowledges funding from the European Union's Horizon 2020 Research and Innovation Programme under the Marie Skłodowska-Curie Grant Agreement No. 847439 and from Corning Inc. (Agreement No. CM00003814). L.E. and H.B. acknowledge FAPESP for doctoral and post-doctoral research fellowships via Process Nos. 2022/01937-5 and 2019/26399-3, respectively. H.E. also acknowledges the CNPq for a Research Productivity grant (No. 310870/2020-8) providing travel support. The authors acknowledge the use of the EPSRC funded Physical Sciences Data-science Service hosted by the University of Southampton and STFC under Grant No. EP/S020357/1.

AUTHOR DECLARATIONS

Conflict of Interest

The authors have no conflicts to disclose.

Author Contributions

L.E. made the crystalline and glassy samples. P.S.S. and A.Z. designed the diffraction project. P.S.S., H.E., E.G.L., and G.J.C. performed the diffraction experiments; P.S.S. and E.G.L. analyzed the results. The solid state NMR experiments were planned, conducted, analyzed, and interpreted by H.B., L.E., and H.E. with input from the diffraction work. P.S.S. devised the structural models and wrote the initial draft of the paper, which was modified after input from all co-authors.

Philip S. Salmon: Conceptualization (equal); Data curation (equal); Formal analysis (lead); Funding acquisition (equal); Investigation (equal); Methodology (equal); Project administration (equal); Resources (equal); Software (equal); Supervision (equal); Validation (equal); Visualization (equal); Writing - original draft (lead); Writing - review & editing (equal). Esther Girón Lange: Formal analysis (equal); Investigation (equal). Anita Zeidler: Data curation (equal); Funding acquisition (equal); Investigation (equal); Methodology (equal); Supervision (equal); Writing - review & editing (equal). Henrik Bradtmüller: Conceptualization (equal); Formal analysis (equal); Investigation (equal); Methodology (equal); Software (equal); Supervision (equal); Validation (equal); Visualization (equal); Writing - review & editing (equal). Laureano Ensuncho: Formal analysis (equal); Investigation (equal); Validation (equal); Visualization (equal); Writing - review & editing (equal). Gabriel J. Cuello: Funding acquisition (equal); Investigation (equal); Supervision (equal); Writing – review & editing (equal). Hellmut Eckert: Conceptualization (equal); Formal analysis (equal); Funding acquisition (equal); Investigation (equal); Methodology (equal); Project administration (equal); Resources (equal); Supervision (equal); Validation (equal); Visualization (equal); Writing - review & editing (equal).

DATA AVAILABILITY

The datasets created during this research are openly available from the University of Bath Research Data Archive at https://doi.org/10.15125/BATH-01565.⁴⁴ The D4c diffraction datasets are available from Ref. 45.

REFERENCES

- ¹R. K. Brow, J. Non-Cryst. Solids **263–264**, 1 (2000).
- ²W. Strojek and H. Eckert, Phys. Chem. Chem. Phys. 8, 2276 (2006).
- ³A. Flambard, L. Montagne, L. Delevoye, G. Palavit, J.-P. Amoureux, and J.-J. Videau, J. Non-Cryst. Solids 345–346, 75 (2004).
- ⁴A. Flambard, J. J. Videau, L. Delevoye, T. Cardinal, C. Labrugère, C. A. Rivero, M. Couzi, and L. Montagne, J. Non-Cryst. Solids **354**, 3540 (2008).
- ⁵D. Manzani, T. Gualberto, J. M. P. Almeida, M. Montesso, C. R. Mendonça, V. A. G. Rivera, L. De Boni, M. Nalin, and S. J. L. Ribeiro, J. Non-Cryst. Solids 443, 82 (2016).
- ⁶L. M. Marcondes, L. Rodrigues, C. Ramos da Cunha, R. R. Gonçalves, A. S. S. de Camargo, F. C. Cassanjes, and G. Y. Poirier, J. Lumin. **213**, 224 (2019).
- ⁷L. M. Marcondes, R. O. Evangelista, R. R. Gonçalves, A. S. S. de Camargo, D. Manzani, M. Nalin, F. C. Cassanjes, and G. Y. Poirier, J. Non-Cryst. Solids **521**, 119492 (2019).
- ⁸P. Mošner, T. Hostinský, and L. Koudelka, J. Solid State Chem. **316**, 123545 (2022).
- ⁹O. C. Gagné and F. C. Hawthorne, Int. Union Crystallogr. J. 7, 581 (2020).
- ¹⁰O. B. Lapina, D. F. Khabibulin, K. V. Romanenko, Z. Gan, M. G. Zuev, V. N. Krasil'nikov, and V. E. Fedorov, Solid State Nucl. Magn. Reson. 28, 204 (2005).
- ¹¹ M. de Oliveira, Jr., H. Damasceno, P. S. Salmon, and H. Eckert, J. Magn. Reson. Open 12-13, 100067 (2022).
- ¹²L. Ensuncho, H. Bradtmüller, P. S. Salmon, and H. Eckert, J. Am. Chem. Soc. 147, 31147 (2025).
- ¹³H. E. Fischer, A. C. Barnes, and P. S. Salmon, Rep. Prog. Phys. **69**, 233 (2006).
- ¹⁴L. V. D. Gammond, H. Auer, R. Mendes Da Silva, A. Zeidler, J. F. Ortiz-Mosquera, A. M. Nieto-Muñoz, A. C. M. Rodrigues, I. d'Anciães Almeida Silva, H. Eckert, C. J. Benmore, and P. S. Salmon, J. Chem. Phys. 155, 074501 (2021).
- ¹⁵D. I. Grimley, A. C. Wright, R. N. Sinclair, and J. Non, J. Non-Cryst. Solids 119, 49 (1990).

- ¹⁶A. C. Hannon, PFIT correlation function fitting software (2023), http://alexhannon.co.uk/software/pfit.htm.
- ¹⁷D. R. Sørensen, U. G. Nielsen, and E. M. Skou, J. Solid State Chem. **219**, 80 (2014).
- ¹⁸W. Li, X. Xia, J. Zeng, L. Zheng, and G. Li, Ceram. Int. 46, 3759 (2020).
- ¹⁹ J. Zhou, P. Gong, A. Ji, M. Xia, J. Jin, and Q. Wu, Inorg. Chem. **63**, 8440 (2024).
- ²⁰H. E. Fischer, G. J. Cuello, P. Palleau, D. Feltin, A. C. Barnes, Y. S. Badyal, and J. M. Simonson, Appl. Phys. A: Mater. Sci. Process. **74**, S160 (2002).
- ²¹ P. S. Salmon, S. Xin, and H. E. Fischer, *Phys. Rev. B* **58**, 6115 (1998).
- ²²V. F. Sears, Neutron News **3**, 26 (1992).
- ²³ H. E. Fischer, J. M. Simonson, J. C. Neuefeind, H. Lemmel, H. Rauch, A. Zeidler, and P. S. Salmon, J. Phys.: Condens. Matter 24, 505105 (2012).
- ²⁴G. B. M. Vaughan, R. Baker, R. Barret, J. Bonnefoy, T. Buslaps, S. Checchia, D. Duran, F. Fihman, P. Got, J. Kieffer, S. A. J. Kimber, K. Martel, C. Morawe, D. Mottin, E. Papillon, S. Petitdemange, A. Vamvakeros, J.-P. Vieux, and M. Di Michiel, J. Synchrotron Radiat. 27, 515 (2020).
- ²⁵R. Mendes Da Silva, A. Zeidler, H. Mohammadi, L. V. D. Gammond, E. Girón Lange, R. E. Youngman, B. G. Aitken, A. C. Hannon, C. J. Benmore, G. B. M. Vaughan, and P. S. Salmon, J. Chem. Phys. 159, 064501 (2023).
- ²⁶D. Waasmaier and A. Kirfel, Acta Crystallogr., Sect. A: Found. Crystallogr. 51, 416 (1995).
- ²⁷J. M. Longo, P. Kierkegaard *et al.*, Acta Chem. Scand. **20**, 72 (1966).
- ²⁸ K. E. Johnston, C. C. Tang, J. E. Parker, K. S. Knight, P. Lightfoot, and S. E. Ashbrook, J. Am. Chem. Soc. **132**, 8732 (2010).
- L. Wang, H. Qi, B. Gao, Y. Liu, H. Liu, and J. Chen, Mater. Horiz. 9, 1002 (2022).
 A. McAdam, K. H. Jost, and B. Beagley, Acta Crystallogr., Sect. B: Struct. Sci., Cryst. Eng. Mater. 24, 1621 (1968).
- ³¹ U. Hoppe, L. Delevoye, L. Montagne, M. v. Zimmermann, and A. C. Hannon, Phys. Chem. Chem. Phys. 15, 8520 (2013).
- ³²G. Costentin, M. M. Borel, A. Grandin, A. Leclaire, and B. Raveau, Mater. Res. Bull. 26, 1051 (1991).
- ³³ J. J. Hudgens, R. K. Brow, D. R. Tallant, and S. W. Martin, J. Non-Cryst. Solids 223, 21 (1998).
- ³⁴T. Cardinal, E. Fargin, G. Le Flem, M. Couzi, L. Canioni, P. Segonds, L. Sarger, A. Ducasse, and F. Adamietz, Eur. J. Solid State Inorg. Chem. 33, 597 (1996).
- ³⁵M. R. Cicconi, D. K. Dobesh, B. Schroeder, T. Otsuka, T. Hayakawa, and D. de Ligny, Opt. Mater.: X 18, 100228 (2023).
- ³⁶A. C. Sakowski-Cowley, K. Łukaszewicz, and H. D. Megaw, Acta Cryst. B 25, 851 (1969).
- ³⁷D. Schildhammer, G. Fuhrmann, L. L. Petschnig, K. Wurst, D. Vitzthum, M. Seibald, H. Schottenberger, and H. Huppertz, <u>Inorg. Chem.</u> 56, 2736 (2017).
- ³⁸ A. Flambard, L. Montagne, L. Delevoye, and S. Steuernagel, Solid State Nucl. Magn. Reson. 32, 34 (2007).
- ³⁹ R. Pang, Z. Wang, J. Li, and K. Chen, Materials **16**, 6956 (2023).
- ⁴⁰L. V. D. Gammond, R. E. Youngman, A. Zeidler, B. G. Aitken, and P. S. Salmon, J. Chem. Phys. **156**, 064503 (2022).
- ⁴¹D. L. Serra and S.-J. Hwu, J. Solid State Chem. **98**, 174 (1992).
- ⁴²H. Mohammadi, R. Mendes Da Silva, A. Zeidler, L. V. D. Gammond, F. Gehlhaar, M. de Oliveira, Jr., H. Damasceno, H. Eckert, R. E. Youngman, B. G. Aitken, H. E. Fischer, H. Kohlmann, L. Cormier, C. J. Benmore, and P. S. Salmon, J. Chem. Phys. 157, 214503 (2022).
- ⁴³ A. A. Lipovskii, D. K. Tagantsev, I. E. Apakova, T. S. Markova, O. V. Yanush, M. G. Donato, L. Sirleto, G. Messina, and G. C. Righini, J. Phys. Chem. B 117, 1444 (2013).
- 44 P. S. Salmon and A. Zeidler (2025). "Transition from a phosphate to niobate network structure in vitreous Nb₂O₅-NaPO₃," University of Bath Research Data Archive, Dataset https://doi.org/10.15125/BATH-01565.
- ⁴⁵P. S. Salmon, G. Cuello, H. Eckert, E. Girón Lange, H. Mohammadi, and A. Zeidler (2023). "Unravelling the chameleon-like nature of Mg in silicate glasses," Institut Laue-Langevin (ILL). https://doi.org/10.5291/ILL-DATA.6-05-1054